water

MDPI

Article

Spatiotemporal Evaluation and Estimation of Precipitation of Multi-Source Precipitation Products in Arid Areas of Northwest China—A Case Study of Tianshan Mountains

Xiaoqian Li [1,2], Xinlin He [1,2,*], Xiaolong Li [1,2,*], Yongjun Du [1,2], Guang Yang [1,2], Dongbo Li [1,2] and Wenhe Xu [1,2]

[1] College of Water Conservancy & Architectural Engineering, Shihezi University, Shihezi 832000, China
[2] Key Laboratory of Modern Water-Saving Irrigation of Xinjiang Production & Construction Group, Shihezi 832000, China
* Correspondence: hexinlin2002@163.com (X.H.); 13150401816@163.com (X.L.)

Abstract: In the arid areas of Northwest China, especially in the Tianshan Mountains, the scarcity of meteorological stations has brought some challenges in collecting accurate information to describe the spatial distribution of precipitation. In this study, the applicability of TRMM3B42, GPM IMERG, and MSWEP V2.2 in different regions of Tianshan Mountain is comprehensively evaluated by using ten statistical indicators, three classification indicators, and variation coefficients at different time–space scales, and the mechanism of accuracy difference of precipitation products is discussed. The results show that: (1) On the annual and monthly scales, the correlation between GPM and measured precipitation is the highest, and the ability of three precipitation products to capture precipitation in the wet season is stronger than that in the dry season; (2) On the daily scale, TRMM has the highest ability to estimate the frequency of light rain events, and MSWEP has the highest ability to monitor extreme precipitation events; (3) On the spatial scale, GPM has the highest fitting degree with the spatial distribution of precipitation in Tianshan Mountains, MSWEP is the closest to the precipitation differentiation pattern in Tianshan Mountains; (4) The three satellite products generally perform best in low and middle longitude regions and middle elevation regions. This study provides a reference for the selection of grid precipitation datasets for hydrometeorological simulation in northwest arid areas and also provides a basis for multi-source data assimilation and fusion.

Keywords: TRMM3B42; GPM-IMERG; MSWEP V2.2; Tianshan Mountains; performance evaluation; spatial heterogeneity

Citation: Li, X.; He, X.; Li, X.; Du, Y.; Yang, G.; Li, D.; Xu, W. Spatiotemporal Evaluation and Estimation of Precipitation of Multi-Source Precipitation Products in Arid Areas of Northwest China—A Case Study of Tianshan Mountains. Atacama Desert (Chile). *Water* **2022**, *14*, 2566. https://doi.org/10.3390/w14162566

Academic Editor(s): Stefano Luigi Gariano

Received: 1 June 2022
Accepted: 18 August 2022
Published: 20 August 2022

1. Introduction

Obtaining accurate spatial distribution of precipitation plays an important role in a wide range of fields, including agriculture, ecosystem, and water resource management [1]. However, it is very challenging to obtain high-quality precipitation estimates at an accurate spatial–temporal resolution, especially in high-altitude mountainous areas, where measurements are often insufficient [2–4]. As the largest mountain system in semi-arid and arid regions of Central Asia [5], the Tianshan Mountains play an important role in determining climate processes in the entire Central Asian region and regional climate system [6–8]. As it is far away from the surrounding ocean, Central Asia has little precipitation and a dry climate. The glaciers and snow in the Tianshan Mountains are important water resources in Central Asia and are affected by precipitation changes [5,9–11]. Global warming accelerates the hydrological cycle [12,13]. By changing the redistribution of water energy in the atmosphere, precipitation in the Tianshan Mountains not only has an important impact on climate change in the glacier region but also affects the natural ecological environment and social and economic activities [14–17]. The terrain of this area is

complex, and the altitude difference is large, which results in the high heterogeneity of precipitation in the Tianshan Mountains with elevation [17,18], from low mountain deserts of <100 mm/year to windward slope high mountains of >900 mm/year. However, there are very few observation stations in the Tianshan mountain area. A total of 70% of meteorological stations are located in the low mountain belt and piedmont plain of the northern and southern slopes of the Tianshan Mountains, and there are few stations in the middle- and high-altitude areas [19]. Therefore, the precipitation results of spatial interpolation based on point distribution station data such as Climate Research Unit (CRU) are not absolutely reliable for the hydrological and ecological research of the Tianshan Mountains and dry lands in Central Asia [18].

Over the past few decades, people have made great efforts to develop consistent and reliable high-resolution precipitation datasets on a regional or global scale [20–23]. At present, there are more than 20 global or near-global grid precipitation datasets, and they are constantly updated (http://ipwg.isac.cnr.it/data/datasets.html), which provides important information for hydrological research in the global and data scarce areas (such as Tianshan Mountains). However, these precipitation datasets are uncertain due to the data source itself, the spatial–temporal resolution, and the algorithms used in the data development process [24,25]. Among them, the GPM product was launched in 2014 as an upgrade of TRMM, and currently, there are few studies on the evaluation of its product performance [26]. Duan et al. [25], and Huffman et al. [27], conducted a preliminary comparison of IMERG and TRMM monthly precipitation products. Their research shows that the two products are similar on land. Liu [28] made a further comparison on a global scale and found that IMERG had a significant advantage over TRMM in detecting heavy monsoon rainfall. However, another study in Asia [29] showed that 75% of measuring stations considered IMERG to be worse than TRMM at heavy rain detection. In addition, the Multi-Source Weighted Ensemble Precipitation (MSWEP) recently produced by European researchers [30] has been widely used in ecological/hydrological studies [31–34]. Several studies have shown that the characterization ability of MSWEP to retrieve surface precipitation is often higher than that of TRMM, CMORPH, GPM, and other global precipitation data [34,35]. When precipitation datasets are used as inputs to hydrological simulations [36,37], uncertainties in satellite products may propagate to hydrological variables (such as runoff) [38,39]. Therefore, it is increasingly necessary to evaluate the performance of different source precipitation datasets [40,41] and their impact on hydrological research, selecting suitable precipitation products according to the study area.

In the previous research, the applicability evaluation of precipitation datasets (or other climate data) in high-cold mountainous areas is usually completed through data comparison; that is, the precipitation products are compared with the measured data to identify the rainfall patterns and other characteristics of different time and space [42,43]. For example, Wang [44] and Li [45] et al. took the Qilian Mountains as the research object. In the study comparing the applicability of the Weather Research and Forecast (WRF) reanalysis products with TRMM and the fifth generation of atmospheric reanalysis by the European Centre for Medium-Range Weather Forecasts (ERA5) [46,47], they found that there are great differences in the estimation of annual and seasonal precipitation in different precipitation datasets at high latitudes; Similar conclusions were reached in the Tianshan Mountains [48]. This illustrates the value of cross-comparisons of datasets to provide in-depth details on the performance of precipitation indicators data important for hydrological and climatic studies. However, these evaluations generally have the following shortcomings: (1) Most studies analyze the applicability of precipitation products in the study area based on a short time scale, ignoring the test of the possible characteristics of precipitation in high-altitude mountainous areas over a long time series [11]; (2) The inversion degree of precipitation products on the spatial–temporal heterogeneity of precipitation in the study area is ignored [49,50]. Especially in the Tianshan Mountains, with complex terrain, the spatial and temporal distribution pattern of precipitation is relatively complex. Focusing only on the inversion accuracy of the spatial distribution of

precipitation from satellite data is difficult to reflect the variation trend of the spatio-temporal scale of precipitation and the details of local precipitation in the mountains [51,52]; (3) The lack of analysis on the source mechanism of estimation differences of precipitation products from different sources may not provide a reference for the application of precipitation products in other high-cold mountains with similar geographical conditions [52–55]. Therefore, these assessments are not always available or reliable [24,55].

In addition, the research on different satellite products in the Tianshan area is very limited. Wang used 24 meteorological stations in the Tianshan mountains for comparative analysis and verified the applicability of TRMM monthly precipitation data in the Tianshan Mountains [56]. Ji Xuan et al. verified the performance of TRMM daily precipitation data in the Central Tianshan Mountains by using 15 meteorological stations around the Central Tianshan Mountains [56]. Zhao et al. analyzed the spatial distribution of precipitation in the Tianshan Mountains by using the precipitation estimation method of the TRMM satellite combined with a rainfall gauge [52]. All the above studies show that TRMM data can accurately estimate precipitation in Tianshan Mountains. However, the above assessment is based on the applicability of a single satellite product in the Tianshan region, which limits the selection and comparison of precipitation products.

In previous studies, the whole Tianshan Mountains are often studied as a research area, and there is a lack of discussion on the spatial variability of precipitation in different regions of the Tianshan Mountains [18,57,58]. The area of the Tianshan Mountains is large, and the precipitation has typical spatial multi-scale and nonlinear characteristics. There is no systematic investigation of the precipitation in different elevations and areas in the Tianshan Mountains. Therefore, this study aims to comprehensively evaluate the quality of raster precipitation products from three different sources in the Tianshan Mountains. By taking the measured data of 36 meteorological stations as a comparison, the regional precipitation estimation accuracy of TRMM3B42, GPM-IMERG, and MSWEP V2.2 satellite products was evaluated. The study period is set as January 2000 to December 2019, which is the overlapping period of three satellite missions. Although the number of stations limits the representativeness of the actual precipitation pattern in mountainous areas, this paper discusses the precipitation pattern at different time scales of day, month, season, and year, as well as the spatial scale of the four sub-regions of the Tianshan Mountains, and it is still possible to evaluate whether the multi-source satellite products can reflect the spatial pattern and temporal change of precipitation. The purpose of this study is to improve the understanding of the suitability and uncertainty of satellite precipitation products in the Tianshan Mountains and evaluate whether the upgrading of precipitation products from different sources can improve the ability to capture light and solid precipitation in the Tianshan region of the dry land of Central Asia.

2. Materials and Methods

2.1. Study Region

The Tianshan Mountains system (39°30′–45°45′ N, 74°10′–96°15′ E) straddles the border between China and Kyrgyzstan and is the largest mountain system in central Asia [11]. This study focused on the Tianshan Mountains in China, where some meteorological stations are available (Figure 1a). The Tianshan Mountain area accounts for two-thirds of the total length of the mountain system, with a length of about 1700 km and a central width of about 350 km. Considering the availability of station data and the availability of DEM, part of the Tianshan Mountains in China was selected as the research area; the altitude of the research area varies greatly, ranging from 321 m to 7426 m. The complex topography of mountains and basins makes the region inaccessible to marine airflow, resulting in an obvious temperate continental arid climate, characterized by extreme temperatures in winter and summer and uneven precipitation heights, ranging from <100 mm/year in low mountain deserts to >900 mm/year in windward slopes of high mountains [18,19]. Because of the hydrometeorological conditions and geospatial constraints in the

mountainous area [18], the K-nearest neighbor method [59] was adopted to divide the Tianshan Mountains into 4 sub-regions, as shown in Figure 1b. According to the observed precipitation data from 2000 to 2019, South Tianshan Mountain is adjacent to the Taklimakan Desert in the south. Due to the interception of water vapor by the peaks on the north slope, the average annual precipitation in this area is the least (203 mm/a); The North Tianshan Mountain mainly includes the Ili River Valley and the main peak area in the middle of Tianshan Mountain. The elevation fluctuates greatly (630–5607 m), and it is located on the windward slope. The annual average precipitation is the highest (424 mm/a); The West Tianshan Mountain is located at the mountain confluence, including the highest peak area (7426 m), with annual precipitation of 308 mm/a; The East Tianshan Mountains mainly include the Turpan Hami basin in the east of Tianshan Mountains and some mountains on the north slope. The average altitude is lower than that of the North Tianshan Mountains and the South Tianshan Mountains. Affected by the northwest monsoon in winter, a large amount of precipitation is formed on the north slope, with average annual precipitation between the two (269 mm/a). The spatial resolution of this study is unified as 0.1° grid division (Figure 1b).

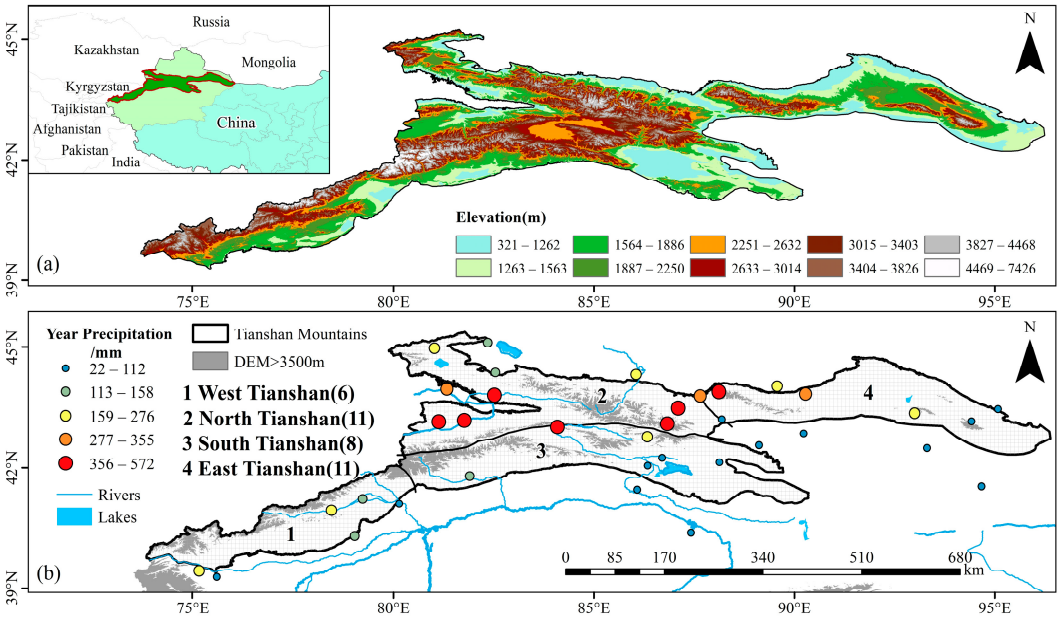

Figure 1. (**a**) Geographical location and Extent and topography of the Tianshan Mountains; (**b**) Boundary of sub–regions, location of stations and their annual precipitation. The number of stations considered for each region: West: 6; North: 11; South: 8; East: 11.

2.2. Data

All the research data in this paper have passed the quality test, and precipitation products used in this study include GPM IMERG, TRMM 3B42, and MSWEP (Table 1). MSWEP is a global precipitation dataset developed by Beck et al. [5], which integrates surface rainfall gauges and a variety of satellites, reanalyzes precipitation information, and corrects it by combining partial runoff and potential evapotranspiration data. MSWEP has the advantages of relatively high spatial resolution (0.1 × 0.1°) and long time series (1979–2017). Despite the high resolution of MSWEP products, MSWEP may not perform as well as TRMM precipitation products in Central Asia and the nearby Tibetan Plateau [34,60]; this may be because the MSWEP fusion algorithm has not fully played its potential to improve the accuracy of precipitation monitoring in some high-altitude areas [32,61], while the TRMM based on microwave algorithm has certain advantages in capturing precipitation particles in the Tibetan plateau [62,63]. In this study, TRMM Version 7 data (3B42V7) with a temporal resolution of 3 h and a spatial resolution of 0.25° were

used. The TRMM product combines multiple satellite observations, including (the first) space-based precipitation radar, infrared and PM sensor data, and precipitation observations from the Global Precipitation Climate Center (GPCC) [60]. The TRMM project was terminated in April 2015 and replaced by the GPM mission. In this study, the IMERG Final Precipitation L3V06 Global Satellite Precipitation Grid dataset was used, which also had the advantage of high spatio-temporal resolution (0.1°, 0.5 h) [64]. The public time span of four datasets (2000–2019) is selected as the research period. The station data involved in this study come from the Information Center of the National Meteorological Administration (http://data.cma.cn/). Among them, considering that the daily precipitation data are the core data for objectively evaluating the performance of remote sensing precipitation products, the researchers screened the stations with intact daily observation precipitation data from 2000 to 2019, and finally, through consistency test and deviation correction [65,66], selected 36 representative weather stations.

Table 1. Data overview.

Dataset	Type	Time Resolution	Space Resolution	Time Range	Coverage	Source
Daily dataset of Surface Climatological Data for China (V3.0)	Observation data from ground stations	1 d	-	1951–-	China	http://data.cma.cn/data/cdcdetail/dataCode/A.0012.0001.html
TRMM3B42	Combined measurements of satellite estimated precipitation	3 h	0.25 × 0.25°	1998–2019	Global	https://gpm.nasa.gov/data/directory
GPM IMERG(V06) Final Run	Multi-satellite joint retrieval of precipitation data	0.5 h	0.1 × 0.1°	2000–	Global	https://gpm.nasa.gov/data/directory
MSWEP (V2.2)	Multi-source fusion of precipitation observation data	3 h	0.1 × 0.1°	1979–2019	Global	http://www.gloh2o.org

2.3. Research Methods

2.3.1. Temporal and Spatial Aggregation of Satellite Precipitation Products

Since the spatial and temporal resolutions of satellite precipitation products used are inconsistent, data need to be aggregated to a unified spatial and temporal resolution for facilitating comparative analysis. In terms of time resolution, because the precipitation product is based on UTC Universal Time [67], and the observation data of meteorological stations are Beijing Time (UTC + 8), the satellite datasets with different time resolutions are converted into Beijing Time by adding 8 h, and then the corresponding time periods are selected and accumulated into daily data. In terms of spatial resolution, all data are unified to 0.1°, in which the 0.25° TRMM3B42 satellite precipitation products are resampling by bilinear interpolation; the resampling method of bilinear interpolation can realize the conversion of information and retain the information of TRMM satellite products to the maximum extent [68]. After unifying TRMM to the same spatial resolution as MSWEP and GPM, all data had to be unified under the same projection and geographic coordinate system (GCS_WGS_1984) through raster calculation, and the unit (mm) of all products was unified through raster calculation. Then, the spatial data of satellite

products with the same coverage as the research area are extracted by ArcGIS tool. When analyzing the monthly and annual precipitation changes, various data with uniform spatial–temporal resolution are cumulatively summed and averaged grid by grid according to time units to obtain data with different time scales.

2.3.2. Comparison of Applicability of Precipitation Products

There are generally two methods to compare the applicability of precipitation products. One is based on the comparison of surface data, the grid data with the spatial resolution of precipitation products are obtained through the spatial interpolation of measured data, and the grid data are used as the real precipitation to evaluate the precipitation products; Second, based on point data comparison, the measured precipitation series of the station are compared with the nearest precipitation product grid data. In this paper, the first method is used to compare and analyze the spatial distribution differences of different precipitation data. In this study, the special spatial interpolation software ANUSPLIN [69] is used to interpolate the precipitation of 36 stations. In recent years, domestic and foreign scholars have mainly used kriging, co-kriging, spline function, inverse distance interpolation, and a variety of statistical regression methods based on geographical spatial characteristics to build software models to fit the spatial statistical characteristics of meteorological elements [70,71]. ANUSPLIN interpolation software is based on partial thin plate smoothing splines [71,72], which introduces influence factors as covariants to build a linear sub-model, and then automatically determines the model coefficients according to the data. It is a relatively mature special meteorological element interpolation tool [69]. The introduction of elevation as a covariate in this study can not only effectively make up for the lack of high-altitude station [73] data but also can interpolate polyhedral spatial data at the same time, especially for long-time series meteorological data [74]. The interpolation results and satellite precipitation results are respectively superimposed for comparative analysis. The second method is used to evaluate the accuracy of multi-time scale precipitation series. Six statistical indexes, including correlation coefficient (CC), frequency bias (BIAS), mean absolute error (MAE), mean error (ME), root mean square error (RMSE), and standard deviation ratio (SDR), are used to reflect the degree of consistency between precipitation products and ground measured data. Probability of detection (POD), false alarm ratio (FAR), and critical success index (CSI) are used to evaluate the recognition ability of precipitation products to daily precipitation events. Coefficient of variation (CV) is used to measure the spatial and temporal variability of precipitation. The calculation formula and optimal value of each indicator are shown in Table A1 of the Appendix A.

CC is used to evaluate the degree of linear coincidence between two kinds of data, which is generally defined as follows: $0.8 < CC \leq 1.0$ means very strong correlation; $0.6 < CC \leq 0.8$ implies a strong correlation; $0.4 < CC \leq 0.6$ means moderate correlation; $0.2 < CC \leq 0.4$ implies weak correlation; $0.0 \leq CC \leq 0.2$ indicates extremely weak or irrelevant [29]; BIAS describes the deviation direction and degree of the forecast model, which can eliminate the influence of precipitation at different stations [31]. MAE can avoid the problem of mutual cancellation of errors and estimate the proximity of satellite products to observation data [32]. ME can use sample statistics to infer the overall accuracy and reflect the systematic error of the data [75]. RMSE reflects the sample deviation between satellite products and observation data and is more sensitive to large errors. SDR reflects the degree of dispersion between data individuals [18]. The higher the POD is, the lower the probability of missing precipitation events is; the lower the FAR is, the lower the probability of precipitation events being wrongly forecast is; the higher the CSI is, the stronger the comprehensive detection ability of precipitation products on precipitation time is. CV is also known as the "standard difference rate", which is the ratio of standard deviation to mean and a statistic to measure the degree of variation of observed variables. In this paper, the coefficient of variation (CV) of annual and seasonal precipitation for each satellite product and measured precipitation grid point in the study area is calculated, which

is used to analyze and compare the spatial distribution of the coefficient of variation of annual and seasonal precipitation.

At present, the 27 core extreme climate indices proposed by the International Expert Group on Climate Change Detection and Indicators (ETCCDI/CRD) are widely applied in identifying hydro-climate extremes [76]. We have selected four of them that are often used to study the characteristics of extreme precipitation [77,78] in high-cold mountains to analyze the extreme precipitation in the Tianshan Mountains (Table A2). They are CDD, CWD, SDII, and RX1D. CDD refers to the longest consecutive days with daily precipitation less than 1 mm, which can effectively reflect the continuous drought in the study area. CWD refers to the longest consecutive days with daily precipitation greater than or equal to 1 mm, which is very important to reflect the wetness of the study area [79,80]. RX1D represents the maximum daily precipitation in a year, which reflects the possibility of extreme precipitation in a year to some extent [80,81]. SDII refers to the ratio between the total amount of precipitation greater than or equal to 1 mm and the number of days, which can reflect the ordinary daily precipitation intensity [79,81].

2.3.3. Comparison Method between Satellite Data and Rainfall Station Data

Referring to the methods of Zambrano et al. [82] and Sharifi et al. [83], the "site-pixel" method was used for comparative analysis of satellite precipitation products and site observations. It can be divided into the following three situations: (1) when the rainfall station completely falls on the pixel of the satellite image grid, the station data and the image metadata are directly used for comparison; (2) When the rainfall station falls between two pixels or the Angle between four pixels (edge < 0.01°), the mean values of two pixels or four pixels were compared with the rainfall station data; (3) When there are two or more rainfall stations in a pixel, the average value of all stations in the pixel is calculated and compared with the value of the pixel.

3. Results

Precipitation has obvious spatial–temporal differences. The applicability and accuracy of precipitation satellite data are mainly reflected in its sensitivity and accuracy in capturing the spatial–temporal differences of precipitation. Therefore, this study will compare the three precipitation satellite data (TRMM3B42 product is resampled with 0.1° resolution, GPM IMERG satellite product, and MSWEP) with the measured data of meteorological stations from two perspectives of time and space, respectively, and analyze their applicability in the Tianshan Mountains. On the time scale, the estimation accuracy of precipitation satellite products will be analyzed from three scales of year (includes wet and dry seasons), month (includes the four seasons), and day. On the spatial scale, the spatial variation of satellite precipitation estimation accuracy in different regions of the mountain area and the influencing factors of the estimation accuracy are mainly analyzed.

3.1. Precipitation Estimation Accuracy at Different Time Scales

3.1.1. Annual Scale Accuracy Assessment

Due to the significant difference in annual variation of precipitation in the Tianshan Mountains [12,13], according to the application of the index station method [84,85], and with reference to the annual distribution of multi-year average precipitation and consecutive maximum precipitation months of representative stations in the Tianshan Mountains [18], the wet season is determined from April to August, and the dry season is determined from September to March of the next year. The index station method is by selecting observation stations that cover the whole study period and have almost no lack of measurement; the wet season is divided according to the monthly average precipitation of each station during the study period [86,87]. This section evaluates the different performances of the three precipitation products in wet and dry seasons; the annual, wet, and dry season precipitation of TRMM, GPM, and MSWEP are evaluated on an annual scale.

This section analyzes the applicability of the three products in the Tianshan Mountains based on the ground measured point data and the corresponding grid point data extracted from precipitation products. SDR, CC, and RMSE of the three precipitation products relative to the observation data of meteorological stations are plotted using the Taylor chart (Figure 2). Based on the annual, wet and dry season precipitation data of 36 stations, the average value of performance indexes of multiple stations in different areas of the Tianshan Mountains was calculated, and the Taylor diagram that could comprehensively reflect SDR, CC, and RMSE was drawn. The position of each point on the Taylor diagram indicates the degree of matching between satellite precipitation product data and precipitation of ground rainfall stations. As shown in Figure 2, the distance from the precipitation product dot to the origin in the figure represents the SDR of the data. The distance between the precipitation product dot and the observation site is the RMSE of the precipitation product data relative to the observation value (which has been normalized). The intersection of the extension line of the origin and precipitation product dot with the 1/4 circle is the CC of precipitation products and observed value [88]. CC cannot objectively reflect the degree of difference in precipitation values measured by satellite products and rainfall stations. Therefore, BIAS and MAE between them should be considered, as shown in Table 2.

From different time scales, the three precipitation products showed a strong correlation with the wet season observation data in most areas of the Tianshan Mountains (West, North, and South), with CC generally greater than 0.8. The annual scale came in second place; CC was the worst in the dry season. MAE also showed that the three products are very close to the measured data in the wet season, but the difference is large in the dry season. The performance differences of the three precipitation products are as follows, as can be seen from Figure 2; in most cases, the distance between the dots of the three precipitation products and the observation stations from near to far is GPM, MSWEP, and TRMM, which also indicates that the order of accuracy of the three in capturing the annual precipitation in Tianshan Mountains is GPM > MSWEP > TRMM.

From different regions, the correlation between the three precipitation products and the measured data at the annual scale has some similarities (Figure 2). All the products had higher correlation coefficients (CC > 0.8) in the West with abundant precipitation and flat terrain. In the South and North, where the height difference changes greatly, it ranks second. The correlation was lower (CC < 0.7) in the East with large terrain fluctuation. BIAS reflects that TRMM and GPM generally underestimate precipitation in different regions at different times, and MSWEP reflects a similar overestimation of measured precipitation at annual and dry season scales. On the other hand, among the three products, MSWEP has the most accurate description of precipitation differentiation in different regions, and SDR is generally greater than 0.9. However, the SDR of GPM is less than 0.7 in the annual and wet seasons, which is lower than the other two, indicating that its description of precipitation variation range needs to be improved. It can be seen that the precipitation in the Tianshan Mountains has the characteristics of uneven spatial and temporal distribution [59], which leads to the differences in the applicability of satellite products at different time scales and different spatial scales. The accuracy evaluation of the annual scale range can only reflect the general characteristics of the three products, and the smaller time scale (monthly scale and daily scale) can help to achieve a more detailed and multi-dimensional accuracy evaluation.

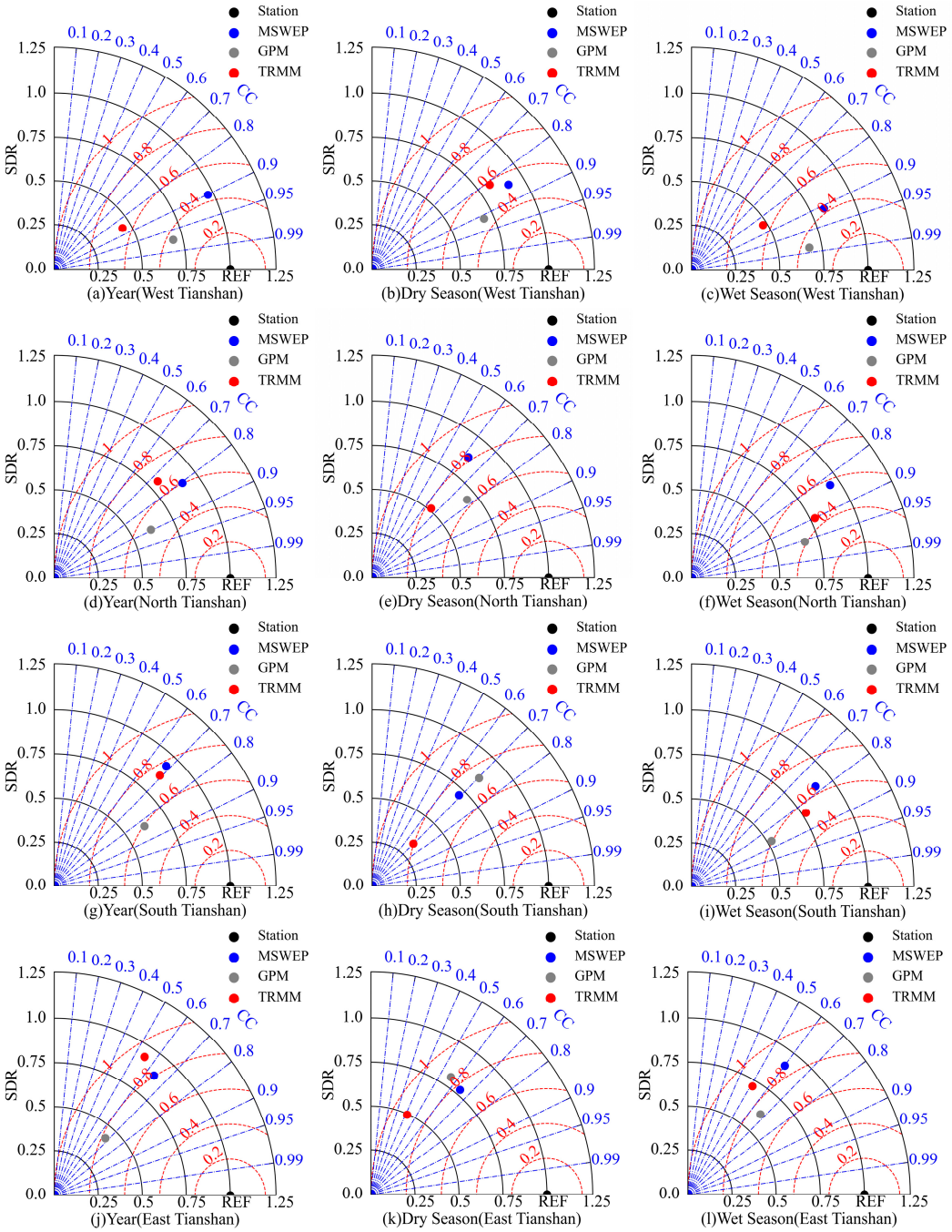

Figure 2. Evaluation indicators Taylor diagram of precipitation products in different regions of annual scale (**a**,**d**,**g**,**j**), dry season (**b**,**e**,**h**,**k**) and wet season (**c**,**f**,**i**,**l**). West Tianshan (**a**,**b**,**c**); North Tianshan (**d**,**e**,**f**);South Tianshan (**g**,**h**,**i**);East Tianshan (**j**,**k**,**l**).

Table 2. Annual scale evaluation indexes of precipitation products BIAS and MAE.

Time Scale	Product	BIAS/%				MAE/mm			
		West	East	South	North	West	East	South	North
Wet Season	TRMM	−7.58	−9.58	−5.89	−9.69	18.09	15.03	47.77	35.48
	GPM	−3.27	−7.87	−8.90	−3.36	18.48	41.37	59.84	46.84
	MSWEP	−9.22	−5.82	−4.83	2.99	20.53	41.36	66.24	66.75
Year	TRMM	−15.08	−17.41	−17.31	−10.88	27.88	32.03	89.67	36.71
	GPM	−5.48	−10.71	−9.50	−5.07	36.78	80.72	67.87	52.75
	MSWEP	1.23	10.95	15.33	19.66	41.71	62.38	69.79	68.48
Dry Season	TRMM	−18.25	−20.82	−19.86	−15.67	68.15	128.35	107.84	92.46
	GPM	−14.56	−15.36	−15.78	−10.85	56.55	126.95	175.88	98.76
	MSWEP	7.54	18.82	29.32	32.85	75.90	74.76	123.05	144.76

3.1.2. Monthly Scale Accuracy Assessment

In this section, daily precipitation is accumulated on a monthly scale based on point data to evaluate the accuracy of precipitation products. Figure 3 shows the distribution of main error evaluation indexes of monthly precipitation grid data of TRMM, GPM, and MSWEP in each region. As can be seen from Figure 3, the correlation degree between the three precipitation products and measured precipitation in different regions is in descending order: West region > South region > East region > North region. TRMM (CC = 0.78) and MSWEP (CC = 0.83) perform best in Southern region, and the CC of GPM is as high as 0.95 in West region. Compared with TRMM and MSWEP, GPM here shows greater advantages in the correlation coefficient with the measured precipitation than the annual mean scale (Figure 2). The reason may be that the orbit inclination of the GPM satellite has increased from 35° to 65°, which not only expands the detection coverage area but also improves the product time resolution [89]. Compared with the small fluctuation of the average precipitation for many years, the precipitation in Tianshan Mountains has the characteristics of uneven distribution within the year [50]. Therefore, GPM products can show more detection advantages on a monthly scale. Except that MSWEP shows a certain degree of overestimation in the North, the BIAS of the three data shows an underestimation of the measured precipitation, which has similar characteristics to the BIAS change pattern of the wet season precipitation of the three products (Table 2), which may be because the annual precipitation of Tianshan Mountain mainly comes from the wet season [7]. In order to further analyze this intra-year difference, Figure 4 compares the monthly distribution of the main error evaluation indicators corresponding to TRMM, GPM, and MSWEP precipitation products (average value from June 2000 to December 2019).

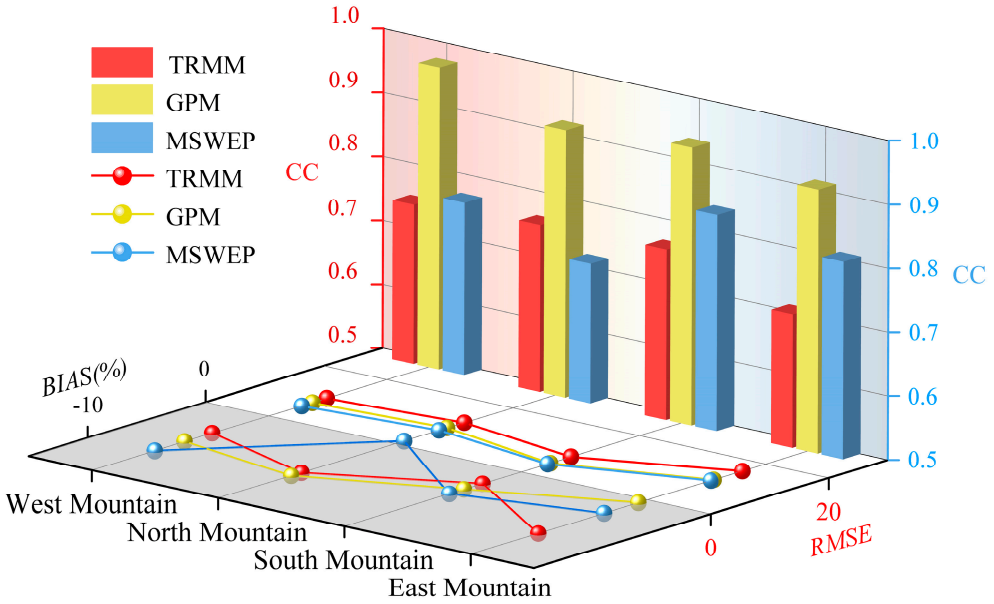

Figure 3. Comprehensive analysis of CC, BIAS and RMSE for monthly scale evaluation of precipitation products.

As can be seen from Figure 4, all satellite products correctly reflect the general pattern of annual variation of precipitation observed at each monitoring station during the study period. RMSE and MAE of the three products generally present a u-shaped distribution in each month of the year, with the lowest values from June to August (RMSE < 10, MAE < 10). This shows once again that the three precipitation products have good detection rates for wet season precipitation events in the year. In the dry season (September to March of the next year), the detection rate was worse (RMSE > 15, MAE > 20).

The deviations of the three products varied greatly in each month of the year, but the estimation ability of the three products showed the same seasonal characteristics: the three sets of products all showed slight underestimation of spring and summer precipitation (average BIAS value from March to August: TRMM: −1.8%; GPM: −1.2%; MSWEP: −0.5%); TRMM, GPM, and MSWEP seriously underestimated and overestimated the precipitation in winter respectively (average BIAS from December to January: TRMM: −6.2%; GPM: −5.8%; MSWEP: + 5.1%). This is consistent with the results that the three products in Table 2 show underestimation of wet season precipitation in most regions (BIAS < 0) and different BIAS of dry season precipitation (TRMM, GPM < 0; MSWEP > 0). The RMSE of the three sets of products was also low in summer and relatively high in winter and spring (Figure 4). In general, the estimation ability of precipitation of the three sets of products was different with the change of season. In winter and early spring, the study area is mainly affected by the Siberian air mass [1,60], and the weather is dry and cold, which is manifested as micro-precipitation and snowfall with very small intensity. In addition, the year-round snow cover in the high-altitude mountainous area causes great interference to the detection of precipitation by microwave-based satellite products [60,65]. In summer and autumn, air masses with moisture from the Atlantic Ocean flow over the complex terrain of the Tianshan Mountains, forming convective rain with heavy rainfall intensity, especially in summer, when the satellite products can better capture the summer precipitation when there is less snow and ice cover.

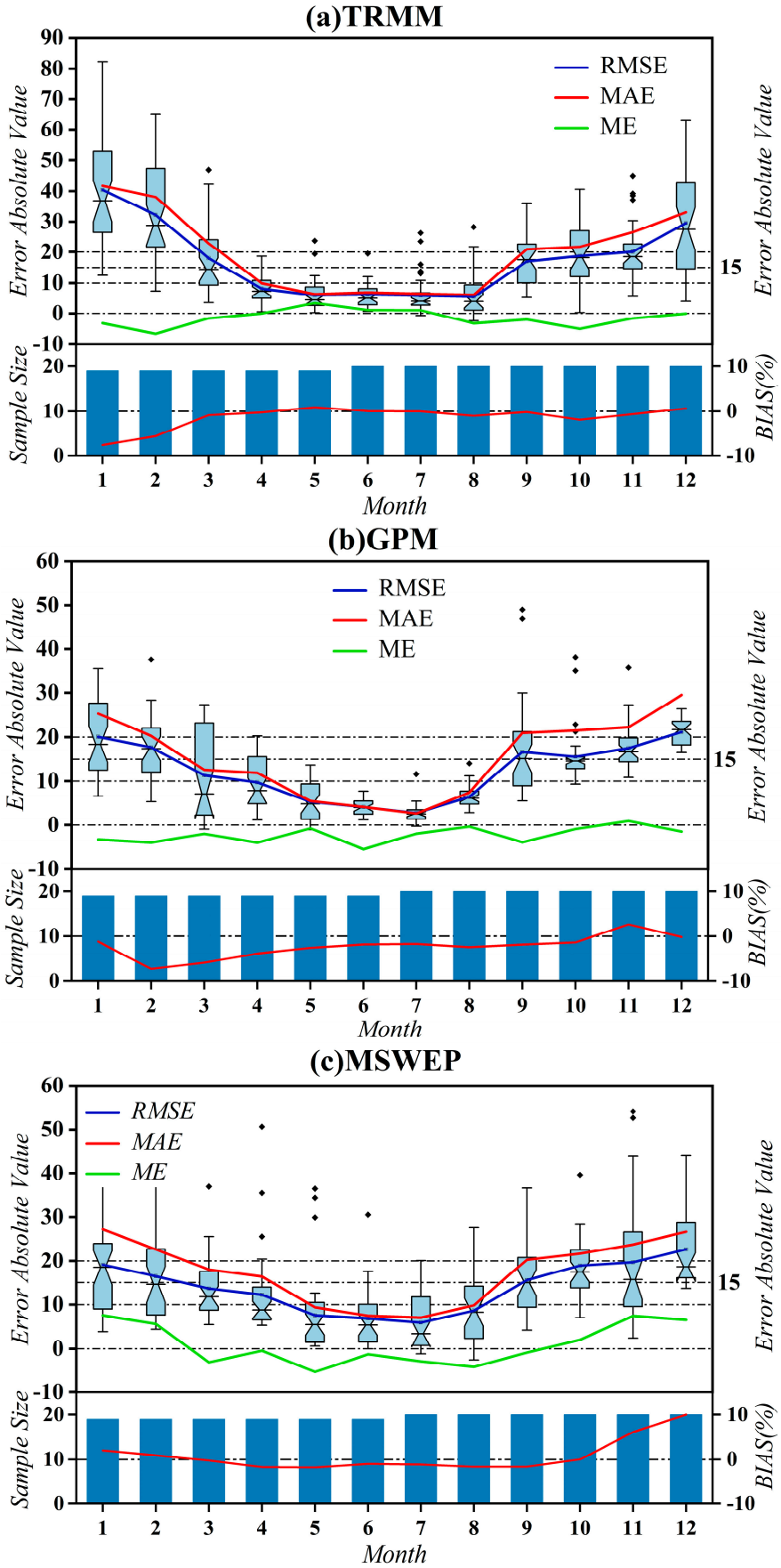

Figure 4. Comprehensive analysis of long-term monthly precipitation error indicators RMSE, MAE, ME and BIAS of (**a**) TRMM, (**b**) GPM and (**c**) MSWEP. In the box plot, the solid black line represents

the median value of RMSE, the square represents the average value, respectively, and the black point represents the outliers.

3.1.3. Daily Scale Accuracy Assessment

Based on point data, POD, FAR, CSI and BIAS are used to evaluate the estimation accuracy of daily precipitation events for three precipitation products in different areas of the Tianshan Mountains.

Figure 5 shows the box diagram of the spatial distribution of POD, FAR, CSI, and BIAS of the precipitation products of each satellite for the observed values of meteorological stations in each region. From the perspective of the whole research area, the FAR of each satellite product shows an increasing characteristic from southwest to northeast, and POD and CSI generally show a decreasing trend from southwest to northeast. In the Western, Southern, and Eastern regions, MSWEP has the lowest FAR, especially in the relatively arid Eastern region, which has a large gap compared with other products, proving that rare precipitation in arid regions is difficult to be detected, while MSWEP has an outstanding ability to detect a small amount of precipitation in arid regions, and GPM has a higher FAR than TRMM and MSWEP in different regions, indicating that it has a higher probability of incorrectly predicting precipitation events. Compared with the other two products, the POD and CSI values of MSWEP in each climate region are significantly closer to the optimal value 1, indicating that MSWEP has higher accuracy, especially the CSI is much higher than other products. On the whole, MSWEP is obviously superior to the other two products in precipitation classification performance. Although GPM shows a high probability of the wrong prediction of daily precipitation events on FAR, at the same time, the POD of TRMM in different zones is not as good as the other two products, and its error index range changes greatly (the box size reflects the data range), indicating that the detection ability of TRMM and GPM for daily precipitation events is not very different. As shown in Figure 5, the data basically conform to a normal distribution, so the obtained law has a certain credibility.

However, POD and CSI are mainly used to evaluate the recognition ability of precipitation products for daily precipitation events, and there is a lack of research on the deviation between precipitation products and measured daily precipitation values [64]. Therefore, BIAS is used in this section to reflect the deviation degree of precipitation products from the measured daily precipitation. As can be seen from Figure 5, although MSWEP can accurately estimate daily precipitation events, it overestimates daily precipitation to varying degrees in most regions (West, South, and North) and slightly underestimates it in East. In different regions, GPM products improved the underestimation of TRMM products to some extent, and compared with MSWEP, GPM was closest to the measured daily precipitation values.

Based on the performance of the three products under the four indicators, we find that the estimation error of GPM for daily precipitation values is relatively low, which is consistent with the accuracy comparison results in the annual scale (Figure 2) and the monthly scale (Figure 3); MSWEP shows relatively high detection ability for the occurrence of daily precipitation events, which may be due to the fact that there are a large number of extreme precipitation events in the Tianshan Mountains in the northwest arid region [90]. MSWEP adopts a Budyko-based framework and global runoff observation to help it monitor precipitation events that are not easy to capture [91].

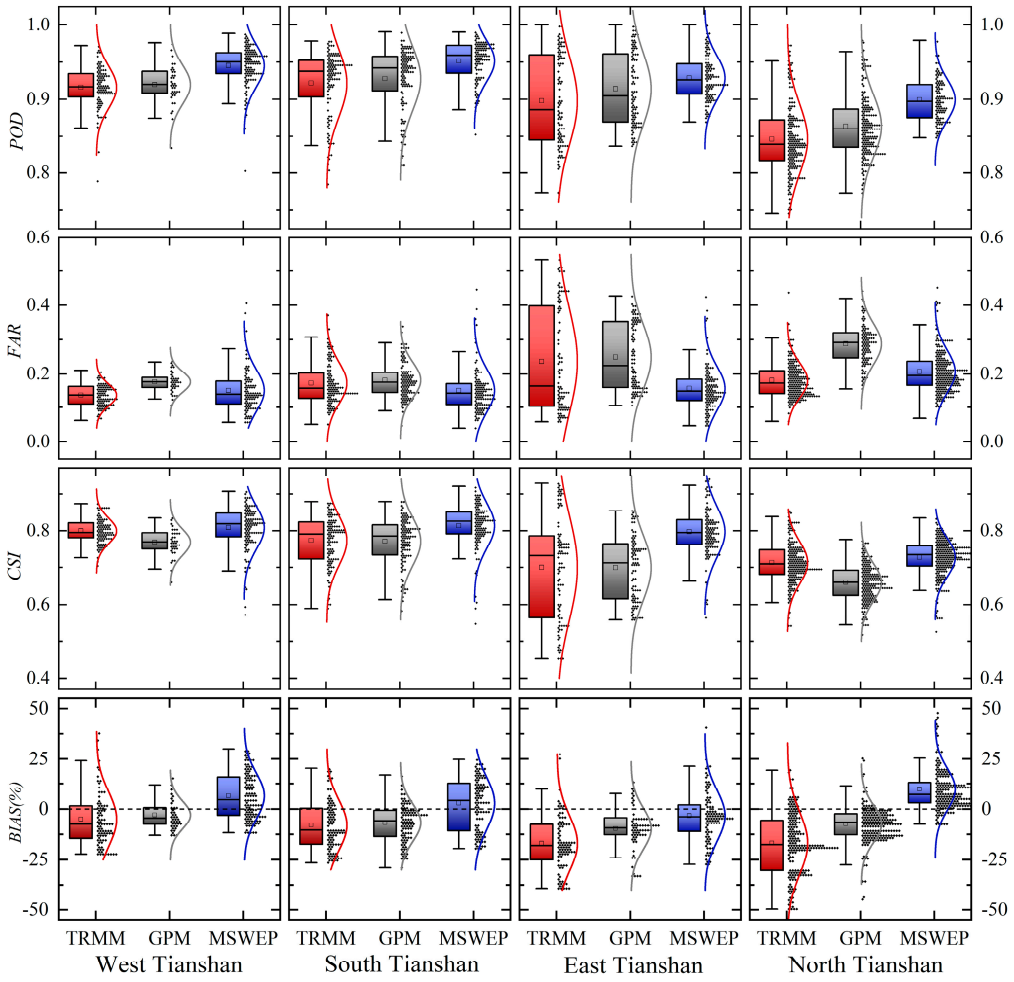

Figure 5. Statistical analysis of POD, FAR, BIAS and CSI of different precipitation products in different regions. In the box plot, the solid black line represents the median value, the square represents the average value, and the four horizontal lines from top to bottom are the upper edge line, upper quartile, lower quartile, and lower edge, respectively, and the hollow black point represents the outliers, and the scatter and curve reflect the normal distribution of data.

3.1.4. Comparison of Frequency Distribution of Precipitation Intensity

In order to further test the different detection capabilities of precipitation products for daily precipitation events, we compared the frequency distributions of daily precipitation with different intensities. Figure 6 shows the precipitation data of all stations and the distribution of each dataset in different rainfall ranges. Rainfall classification is based on the classification standard of precipitation intensity grade issued by the National Meteorological Administration [54]. TRMM, GPM, and MSWEP underestimated the days without rain in the study area (4.6~14.3% and −13.7~19.2% and 9.5~12.6%) in different regions; However, the number of light rain days was overestimated in different degrees (+4.8% to +16.1%, +15.4% to +22.7% and +9.9% to +15.0%). For moderate rain and rainstorm, except that GPM in Western Tianshan overestimates the number of moderate rain days (+0.28%), satellite precipitation is underestimated to varying degrees in other cases; MSWEP is the best for rare heavy rain and above precipitation. GPM precipitation products can occasionally monitor extreme precipitation, while TRMM precipitation products can not be detected in all regions. From the perspective of each region, except the Eastern part of the Tianshan Mountains, TRMM performed best in detecting the frequency of rainless events, followed by MSWEP and GPM (the average difference with the observation is: TRMM (5%) < MSWEP (15%) < GPM (25%). MSWEP performs better than TRMM and GPM (the average difference with the observation is: MSWEP (10%) < TRMM (15%) < GPM (20%)). in the detection of precipitation frequency of different magnitude in the Eastern Tianshan region with scarce precipitation, which is consistent with the conclusion from Figure 5 that MSWEP has an outstanding ability to detect precipitation in the arid region.

In general, TRMM performed best in estimating the frequency distribution of days with no rain and days with light rain. MSWEP has the best performance for a rainstorm and superior precipitation. As for the precipitation of moderate rainfall level, the frequency of the three products is not very different.

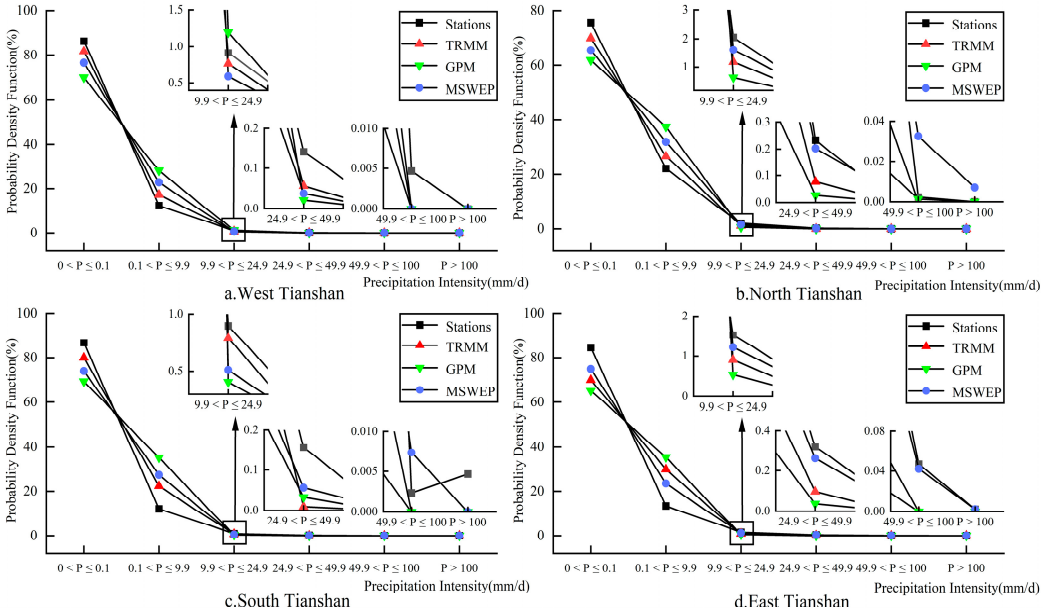

Figure 6. Frequency distribution of daily precipitation of different magnitudes in (**a**) West Tianshan, (**b**) North Tianshan, (**c**) South and (**d**) East Tianshan.

3.1.5. Evaluation of Extreme Precipitation Monitoring Capability

In the 21st century, the northwest arid region has changed from warm and dry to warm and wet [90], and the frequency of extreme precipitation in the Tianshan Mountains has increased [7]. Therefore, the monitoring ability evaluation of extreme precipitation is

also necessary for the applicability comparison of precipitation products on a daily scale. In order to analyze the monitoring ability of TRMM, GPM, and MSWEP for extreme precipitation events during the study period (2000~2019), RClimDEX software [92] is used to calculate the extreme climate indices of satellite observation data of ground observation stations and corresponding grid points site by site. Figure 7a–l shows the scatter density correlation diagram of three satellite products and observation data under each extreme climate indices.

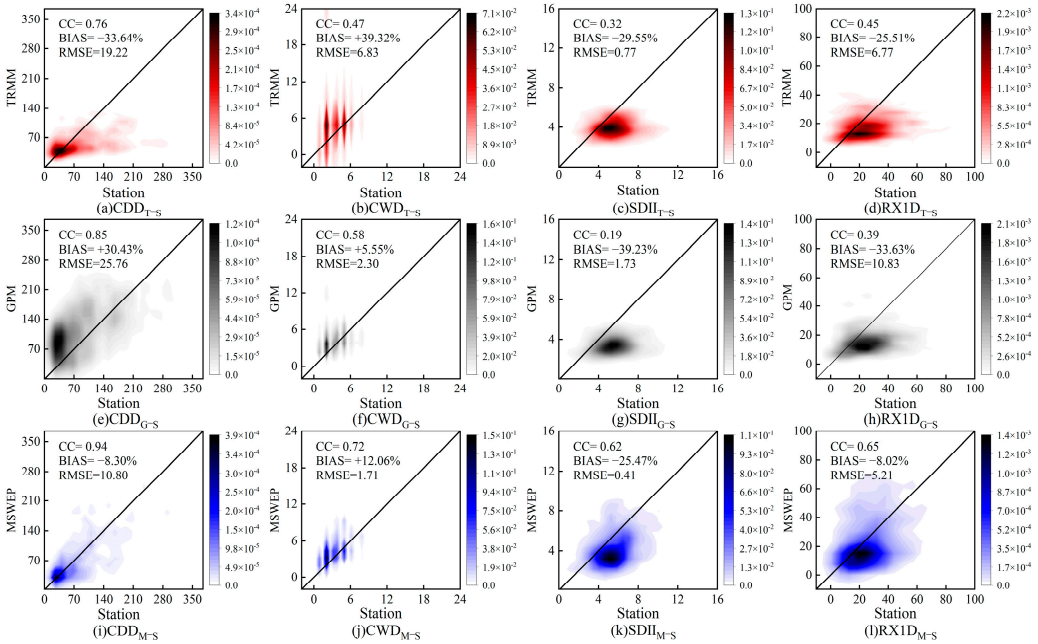

Figure 7. Density scatter of four extreme precipitation indices CDD (**a**,**e**,**i**), CWD (**b**,**f**,**j**), SDII (**c**,**g**,**k**) and RX1D (**d**,**h**,**l**) for precipitation products. TRMM (**a**–**d**); GPM (**e**–**h**); MSWEP (**i**–**l**).

The results show that the CC values of the four groups of extreme climate indices of MSWEP products are greater than those of GPM and TRMM products, and the RMSE values of all extreme climate indices of MSWEP products are also smaller than those of GPM and TRMM, indicating that the fitting effect between the extreme climate indices of MSWEP products and the measured values of stations is better, which can better monitor the occurrence of extreme precipitation. For CWD and CDD indexes, the CC value of the CDD of the three products is relatively high, while the CC value of the CWD index is relatively low, and the correlation is relatively poor. In particular, the CC value of CWD in TRMM products is 0.47, indicating that the number of days of continuous wetting analyzed by TRMM products will be very different from the actual situation, and the results are not of reference significance; For SDII and RX1D indexes, the BIAS of the three products is less than 0, which shows that the precipitation intensity and maximum precipitation are underestimated. Among them, the relatively good performance is that MSWEP slightly underestimates the RX1D index (−8.02%), which can be traced back to the results shown in Figure 6: among the three products, MSWEP has the highest detection rate of precipitation at rainstorm level; The CC of TRMM and GPM products and SDII and RX1D indexes are at a low level (CC < 0.5), indicating that they have little reference significance for regions where extreme precipitation occurs, and surface data are missing.

By analyzing the performance of the three products from the perspective of extreme precipitation monitoring, it can be seen that the monitoring results of MSWEP products for extreme precipitation events are more in line with the actual values. This verifies our conjecture in Section 3.1.3; that is, the high detection ability of MSWEP for daily precipitation comes from the good detection of extreme precipitation events.

3.2. Precipitation Estimation Accuracy at Spatial Scale

3.2.1. Spatial Distribution Characteristics of Precipitation in the Tianshan Mountains

In order to analyze the spatial distribution characteristics of precipitation in the Tianshan Mountains, ANUSPLIN interpolation software [69,93] was used, and three kinds of daily precipitation products were superimposed by the grid. The spatial distribution of precipitation and inter-annual variation coefficient in the measured years (Figures 8a and 9a), dry season (Figures 8e and 9e), and wet season (Figures 8i and 9i) in the Tianshan Mountains, as well as the annual (Figure 8b–d), dry season (Figure 8f–h) and wet season (Figure 8j–l) precipitation distributions and corresponding precipitation differentiation patterns (Figure 9b–d,f–h,j–l) of the three products were obtained. From the perspective of the spatial distribution of annual precipitation, the three precipitation products can roughly reflect the spatial distribution characteristics of measured precipitation, that is, the decreasing trend from northwest to southeast, indicating that satellite products can roughly reflect the spatial differences of precipitation in mountainous areas caused by air flow and topographic changes [37,38]. Here, we integrated the quantity classification in the legend of Figure 8 and the precipitation range of different products, compared the spatial distribution map of different products with the interpolation map of measured precipitation, and roughly obtained the order of magnitude range of differences between products and measured precipitation. The performance differences of the three precipitation products are as follows: TRMM (Figure 8b) underestimates the annual precipitation (379–683 mm) in different regions; MSWEP (Figure 8d) overestimates the precipitation in the South and North regions of the Tianshan Mountains (683–950 mm); GPM (47–727 mm) has improved the underestimation reflected by TRMM to varying degrees in various subregions (Figure 8c), especially in the West (Table 2 can also be seen), which shows a high similarity with the measured annual precipitation (4–726 mm) as a whole. As the distribution of annual precipitation in the Tianshan Mountains is affected by complex geographical location and water vapor sources in different periods (Figure 8d–f), the distribution of precipitation varies greatly in the wet season (Figure 8i) and dry season (Figure 8e); Although the spatial variation range of the precipitation of TRMM (11–262 mm) and GPM (6–364 mm) in the dry season is higher than the measured interpolation result (2–172 mm), BIAS shows that TRMM and GPM generally underestimate the measured precipitation from Table 2 and Figure 4. This difference may come from the fact that Section 3.1 reflects the mean of the stations, which leads to the average of a few high precipitation values (west of the North region) in the dry season in the region. For the dry season precipitation in most regions of the Tianshan Mountains, this underestimation is more common (Figure 8f,g show the general underestimation by TRMM and GPM of precipitation in the 120–172 mm range shown in Figure 8e); TRMM and GPM underestimated the precipitation in the wet season (Figure 8j,k) significantly less than that in the dry season (Figure 8f,g), and MSWEP overestimated the precipitation in the dry season (Figure 8h) significantly higher than that in the wet season (Figure 8l), which is consistent with the conclusion in Figure 2.

From the spatial distribution of CV, the annual precipitation (Figure 9a) and wet season (Figure 9i) precipitation in the Tianshan mountains show low interannual variation ($0 < CV < 16\%$) in most regions. MSWEP is the best reflection of this spatial differentiation pattern among the three precipitation products (Figure 9d,l). For the dry season precipitation with abundant interannual changes ($3 < CV < 57\%$), the differentiation pattern of the three products (Figure 9f–h) is quite different from the measured precipitation. This is consistent with the results of the poor retrieval effect of the three products on the dry season precipitation in the study area (Figure 8e–h). The reason may be that the dry season (September–March) is mainly in winter and early spring, and the snow cover on the mountain surface leads to strong scattering, while the satellite products based on the Microwave algorithm are difficult to distinguish the frozen snow surface and clouds, and even misclassify them into cumulonimbus clouds, which limits the ability of the satellite products to capture precipitation particles. Consistent with the research conclusion of

Feidas, excluding the interference of snow and cold air in winter, satellite products based on infrared sensors can better detect strong convective precipitation in the wet season [22].

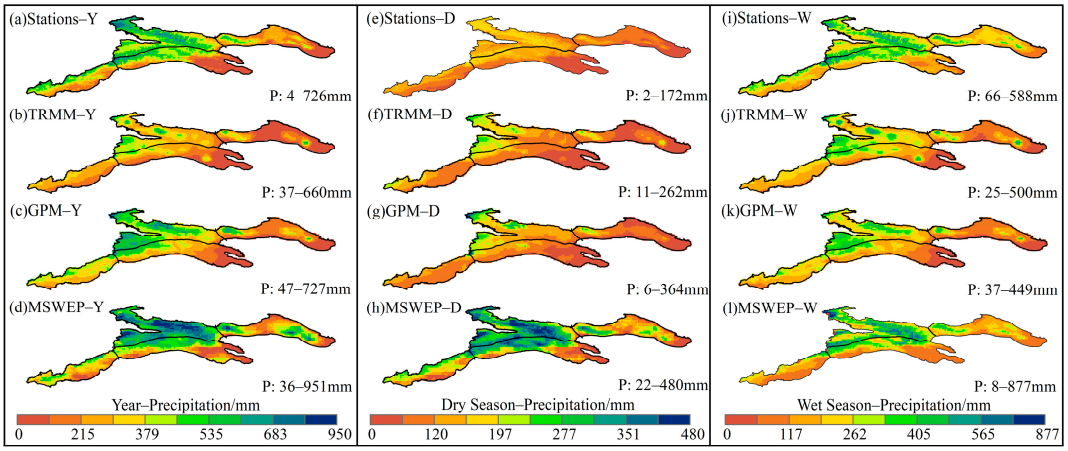

Figure 8. Spatial distribution of precipitation in station interpolation (**a**,**e**,**i**), TRMM (**b**,**f**,**j**), GPM (**c**,**g**,**k**) and MSWEP (**d**,**h**,**l**). Annual scale (**a**–**d**); Dry season (**e**–**h**); Wet season (**i**–**l**).

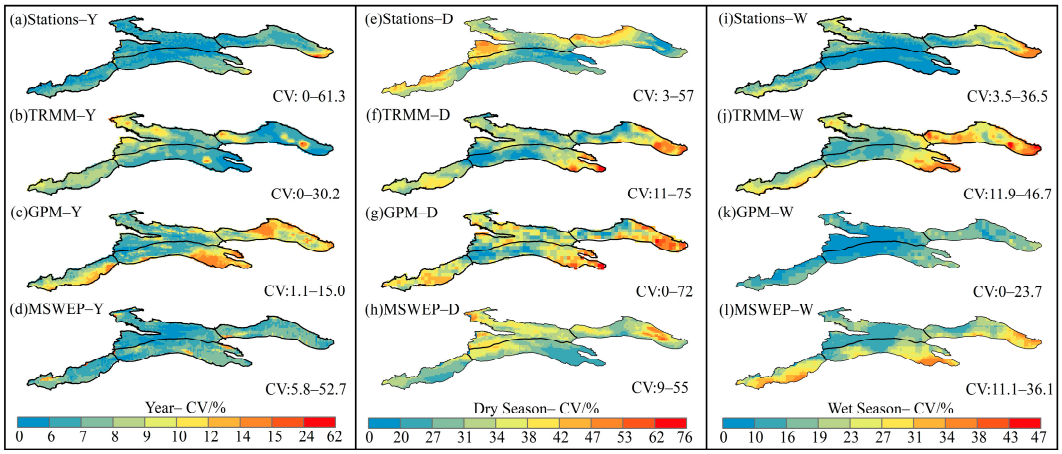

Figure 9. Spatial distribution of CV in station interpolation (**a**,**e**,**i**), TRMM (**b**,**f**,**j**), GPM (**c**,**g**,**k**) and MSWEP (**d**,**h**,**l**). Annual scale (**a**–**d**); Dry season (**e**–**h**); Wet season (**i**–**l**).

3.2.2. Spatial Accuracy Assessment of Precipitation in Tianshan Mountains

In order to further compare the inversion accuracy of the three products on the spatial distribution of precipitation in the Tianshan Mountains, this paper makes a further study on the correlation and error distribution in this section. The satellite annual average precipitation data and the measured annual average precipitation data are compared and analyzed in space, and the distribution map of the relative deviation of satellite precipitation and measured annual precipitation BIAS, CC, and RMSE is obtained (Figure 10). From the perspective of BIAS, the distribution pattern of TRMM and GPM deviations in most regions is similar, ranging from −40% to 20%, showing an underestimation of the measured annual precipitation; The performance differences of the three precipitation products are as follows: GPM has significantly improved the abnormal overestimation of TRMM in a few areas in the South and East regions (50% < BIAS < 100%), indicating that GPM satellite has a better ability to capture precipitation information in the Tianshan mountains than TRMM, which is also reflected in Table 2. The BIAS of MSWEP in most areas is more than 20%, showing an overestimation of the measured precipitation, which is consistent with the research results in Section 3.2.1; in particular, the high-value area in the BIAS distribution pattern of MSWEP is similar to the spatial distribution of dry season

precipitation of MSWEP (Figure 8h), indicating that MSWEP overestimates the measured precipitation mostly from the dry season. The three precipitation products show a strong correlation with the measured precipitation in most areas of the West (CC > 0.8), which is consistent with the conclusion in Figure 2. The sim TRMM, MSWEP and GPM show a correlation from small to large with the measured precipitation in most areas of the northeastern Tianshan Mountains ($CC_T < 0.8 < CC_M < 0.9 < CC_G < 1.0$). In the South region, TRMM and MSWEP show a similar correlation (0.6 < CC < 0.9), and GPM shows abnormal values (CC < 0.6) in the western part of the South, which may be related to the fact that there is only one available station observation value in the western part of the South, and the interpolation results are easy to cause deviation [93]. RMSE is used to highlight the large error in the dataset [17]. GPM (Figure 10h) significantly improves the large error value (RMSE < 30) shown by TRMM (Figure 10g) in most regions of Tianshan Mountain. MSWEP has large error areas (RMSE > 80) in the North, South, and East regions, which may be the reason for its general overestimation of precipitation in different regions of the Tianshan Mountain (Figure 10c). Compared with MAE (Table 2), RMSE can better highlight the widespread overestimation of MSWEP on the annual precipitation in the study area, which indicates that the data must be revised before being applied to further hydrological and meteorological simulation studies.

Through comprehensive comparison, GPM is more in line with the distribution of annual precipitation in the Tianshan Mountains, and MSWEP is more in line with the spatial differentiation pattern of precipitation. In the future, it is considered to combine the two data to improve the estimation accuracy of measured spatial precipitation.

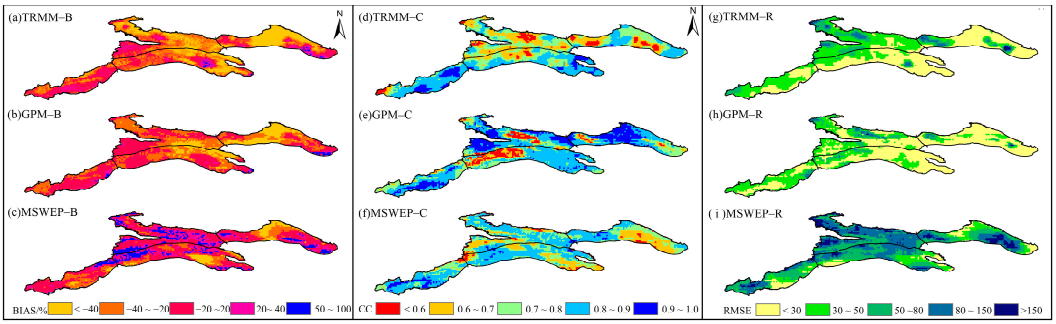

Figure 10. Spatial distribution of BIAS (**a**–**c**), CC (**d**–**f**) and RMSE (**g**–**i**) between precipitation products and measured precipitation interpolation results. TRMM (**a**,**d**,**g**); GPM (**b**,**e**,**h**); MSWEP (**g**–**i**).

3.3. Factors Influencing the Accuracy of Satellite Precipitation Products

Since the Tianshan mountain area is a long and narrow mountain area in the east–west direction, with a large longitude span (74°10′~96°15′ E) and elevation span (321~7426 m), meanwhile, considering the limitation of observation data [11,12] and the special geomorphic structure [18,54] and climatic characteristics of the Tianshan Mountains [50,51,54], elevation and longitude are selected as the influencing factors. The influence of longitude and elevation distribution on the accuracy of satellite precipitation products in the study area is evaluated based on the ground measured point data and the corresponding grid point data extracted from precipitation products.

Based on the observation data, the detectability of TRMM, GPM, and MSWEP to daily precipitation events is evaluated by using POD, FAR, and CSI. Figure 11 shows the spatial distribution of precipitation detection capability indicators at each station. It can be seen that MSWEP has not only the highest POD but also the lowest FAR, so the key success indicator CSI is also the highest at each station: that is, MSWEP has the best detection capability for precipitation events; there is not much difference between GPM and TRMM, which is consistent with the conclusion in Figure 5. The three precipitation products show a poor detection rate for daily precipitation events in low-longitude and low-altitude areas, which may be because satellite products that are in the high-altitude mainly

detect precipitation events at the top of the atmosphere [18,28]. For most low longitude areas (near the Ili River Valley) and other low-altitude areas, the infrared sensors of satellite products may miss precipitation information near the ground, resulting in the omission of precipitation events [94]. It is worth noting that the detection capability of GPM seems to be significantly worse at high-altitudes (Elevation > 2400 m) and Longitude (Longitude > 87° E). The reason may be that the multi-frequency passive microwave imager (GPM microwave imager, GMI) carried by GPM is specially designed for small amounts of precipitation [95], which brings hope to improving the low rainfall intensity overestimation phenomenon in TRMM [60]. However, there is still a lot of room for improvement for the extreme precipitation in high-altitude mountainous areas and the trace or even no rain in high-longitude arid areas (mainly located in the Turpan-Hami Basin in the East region). Therefore, for satellite precipitation assessment in complex terrain and high-altitude areas, more detailed research is still needed to analyze the source of error so as to provide reliable reference information for sensor improvement and algorithm inversion.

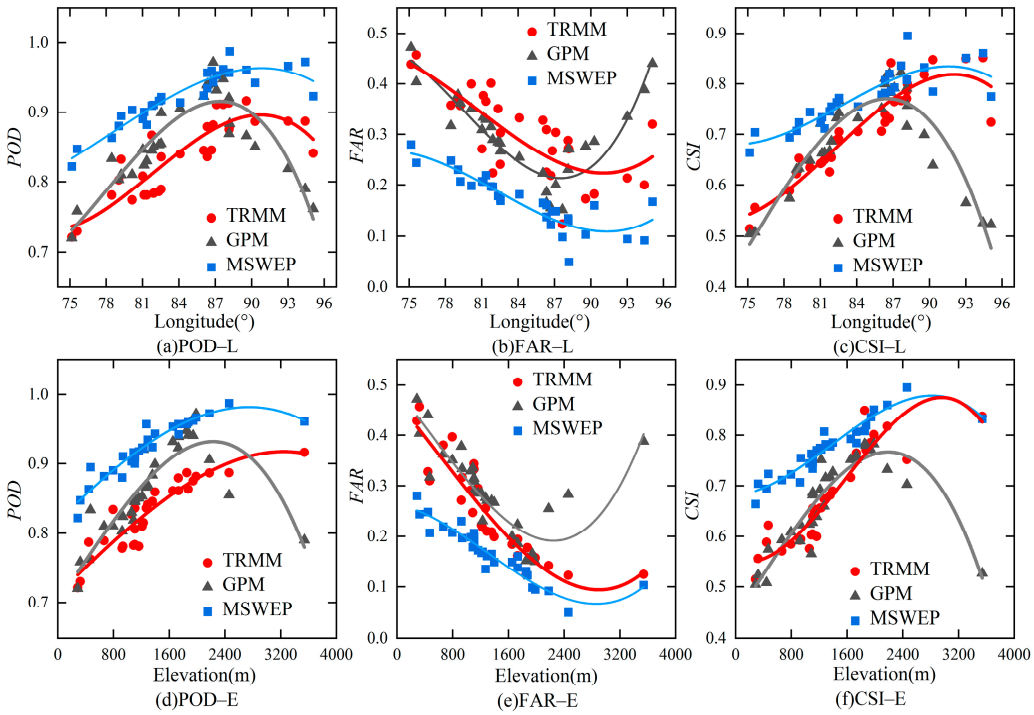

Figure 11. Scatter diagram and fitting lines of daily precipitation detection indicators and longitude (**a**–**c**) and elevation (**d**–**f**) of three products.

In order to further evaluate the influence of topography on the accuracy of precipitation estimation, the spatial distribution of precipitation error was analyzed by combining DEM in the study area. Taking the longitude and altitude of meteorological stations as independent variables and the CC and |BIAS| between the precipitation data of three satellites at different time scales and the measured data of stations as dependent variables, the polynomial regression analysis is carried out. The regression results are shown in Figure 12a–p.

It can be clearly seen that the accuracy indicators of the three products basically have the same trend, but there are some differences in different time scales. The correlation coefficient decreases with the increase in longitude. |BIAS| increase with the increase in longitude. This may be because the low-longitude area mainly covers the West region of the Tianshan Mountains, while the high-longitude area mainly covers the East region of the Tianshan Mountains. The three products have good applicability in the West region with abundant precipitation, while the Turpan-Hami Basin in the East region is far away from the ocean and has closed terrain. The dry and hot subtropical continental air mass makes the weather in the East dry and hot [7], accelerating the evaporation of atmospheric

water. Coupled with the blocking of mountains and the dissipation of air resistance during water vapor transport, it is difficult for water vapor at the top of the atmosphere to completely fall to the ground, resulting in an overall error in precipitation products. This is proved by the accurate evaluation of the Taylor diagram (Figure 2) and the monthly scale evaluation diagram (Figure 3). This is in contrast to the fact that the three products are not dominant in capturing daily precipitation events in low-longitude areas (Figure. 11), possibly because, although some near-surface precipitation events are missed by the satellite product [94], most missed precipitation events are likely to be widespread micro-precipitation events (Figure 6). For the West region with abundant precipitation (the main region of the low-longitude region), satellite products still have good precipitation value detection performance [35,36], especially MSWEP (Figure 12j,k,o), which is good at monitoring heavy rain events (Figure 6). Meanwhile, in the correlation diagram between annual precipitation (Figure 12i) and precipitation in the dry season (Figure 12o), there is a poor correlation phenomenon in some stations in the low-longitude area, which may be due to the large absolute error of precipitation products on precipitation in the West in the dry season (Table 2). The relationship between |BIAS| and elevation basically presents a strong cubic relationship; with the increase in elevation, |BIAS| shows a decrease-increase -less fluctuation change; CC increases with the increase in elevation. Except in the dry season, it reaches a large correlation (CC > 0.75) in the middle- and high-altitude areas (2500–3000 m), which may be because the satellite products detect precipitation information at the top of the atmosphere based on microwave and infrared sensors, rather than the precipitation information near the ground. As a result, precipitation estimates from some satellite products may evaporate before reaching the surface or even not fall to the surface at all [94], resulting in incorrect estimates of precipitation at lower elevations. However, the correlation peak value of precipitation in the dry season decreased to 1500 m above sea level, which may be because the water vapor source in the dry season was mainly dominated by the westerly circulation [18]. It passes through the western section of the North of Tianshan Mountains to form the main precipitation in the dry season (Figure 8e), and the high precipitation value in this region was captured by the three products (Figure 8f–h). During the wet season, the westerly circulation moves northward [18], causing a lot of precipitation. The western section of the North region is mainly distributed in plain areas and near river valleys (with a lower altitude), while the northern section is located in peak gathering area (with a higher altitude), indicating that the three products are also sensitive to the identification of the maximum precipitation altitude zone. For the micro precipitation in high-altitude mountainous areas, although GPM shows a low detection rate for daily precipitation events (Figure 11), the V06 version of IMERG, based on the optimization of the system algorithm and the upgrading of the sensor level, improves the estimation error of the micro precipitation in a long-time scale (month, year) [46,96].

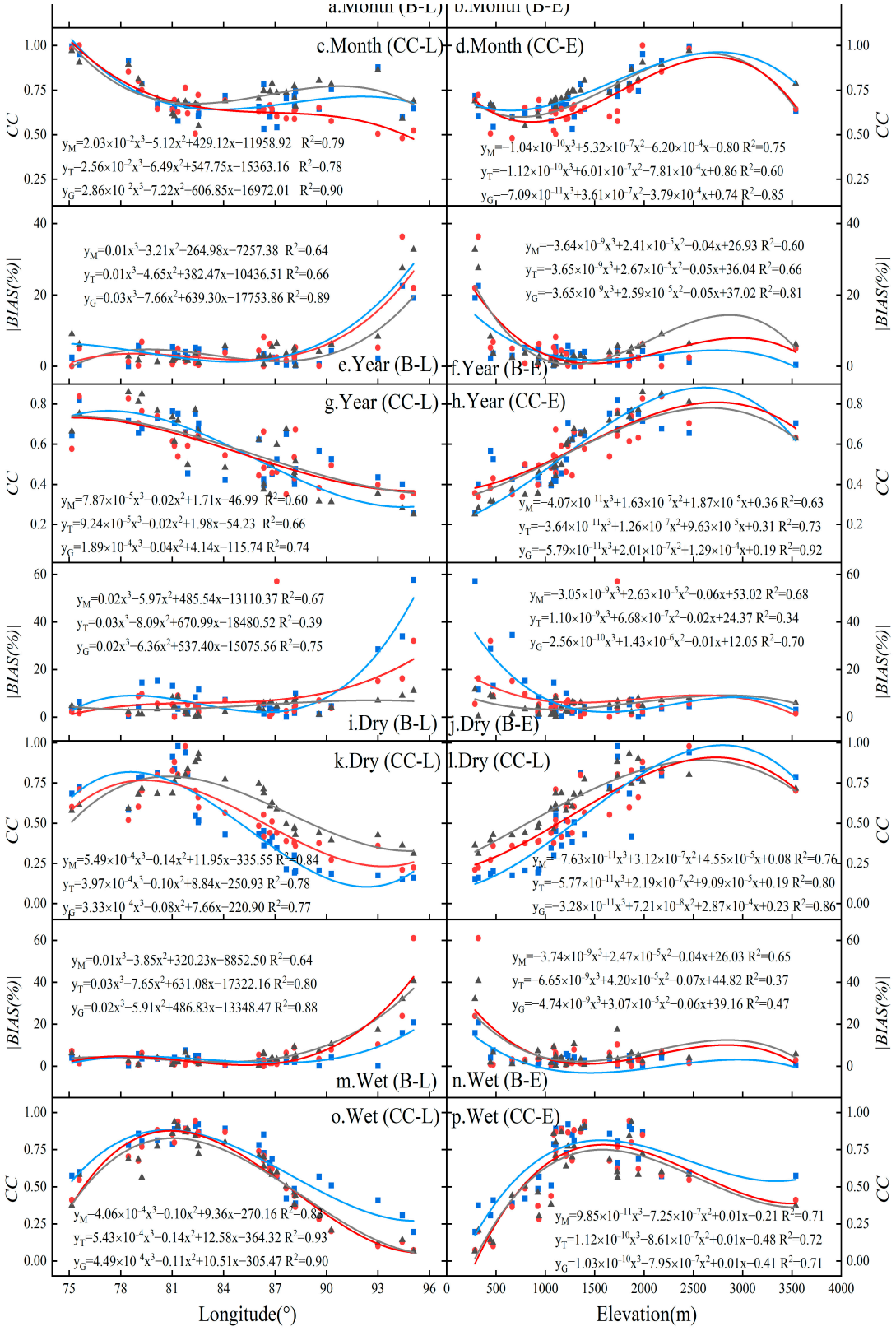

Figure 12. Scatter correlation diagram and fitting lines of monthly, annual, dry and wet season precipitation detection indicators and longitude (**a**,**c**,**e**,**g**,**i**,**k**,**m**,**o**) and elevation (**b**,**d**,**f**,**h**,**j**,**l**,**n**,**p**) of the three products. Monthly scale (**a**–**d**); Annual scale (**e**–**h**); Dry season (**i**–**l**); Wet season (**m**–**p**).

The elevation range of the stations selected in this study is 179–3539 m, and the elevation range of the study area is 321–7426 m. Although the research conclusion has some limitations, it still describes the variation law of precipitation product accuracy with

topography to a certain extent. In conclusion, the deviation between the three products and the measured precipitation is small in the low and middle longitude areas, and the correlation between the three products and the measured precipitation is strong in the middle-altitude areas. This may be because the high longitude and altitude areas in the study area have been iceberg areas for many years [18,54], and most solid precipitation exists, indicating that TRMM, GPM, and MSEWP are similar to most satellite precipitation inversion products, their estimation ability of solid precipitation is still insufficient [14]. However, compared with the three, GPM, as an up-graded product of TRMM, has a better ability to estimate the annual precipitation in low- and middle-altitude areas (Figure 12j,l). MSWEP performs relatively well at high altitudes. In order to further verify the correlation between different precipitation products and measured precipitation in different altitude ranges, this study uses the natural breakpoint method [97] to grade the station elevation and uses the classification results to conduct zoning statistics on the three products and the multi-year average measured precipitation, as well as the CC and BIAS, and obtain the statistical values of different elevation ranges (Figure 12). According to the natural breakpoint method and the elevation range of the station, the low-altitude area is divided into 179–738 m, the medium-altitude area is divided into 739–1574 m, and the high-altitude area is 1575–3539 m.

It can be seen from Figure 13 that the three products all show high CC (TRMM: 0.79; GPM: 0.88; MSWEP: 0.74) and low BIAS (−1.34%, −0.86%, +3.79%) with the measured precipitation in the middle-altitude mountainous areas, indicating that the three sets of precipitation products have good applicability in the middle-altitude areas. This is basically consistent with the results in Figure 11. With the increase in altitude, TRMM and GPM tend to underestimate precipitation. However, compared with TRMM, GPM significantly improves the underestimation of measured precipitation; MSWEP shows overestimation of measured precipitation in different altitude areas, but it shows higher accuracy than TRMM and GPM in high-altitude areas (CC = 0.92, BIAS = +3.5%), which may be due to the scarcity of station data in high-altitude areas. As a multi-source product integrating station network density, satellite precipitation inversion accuracy, and numerical prediction of precipitation results [30], MSWEP reduces the estimation error of precipitation in high-altitude areas accordingly.

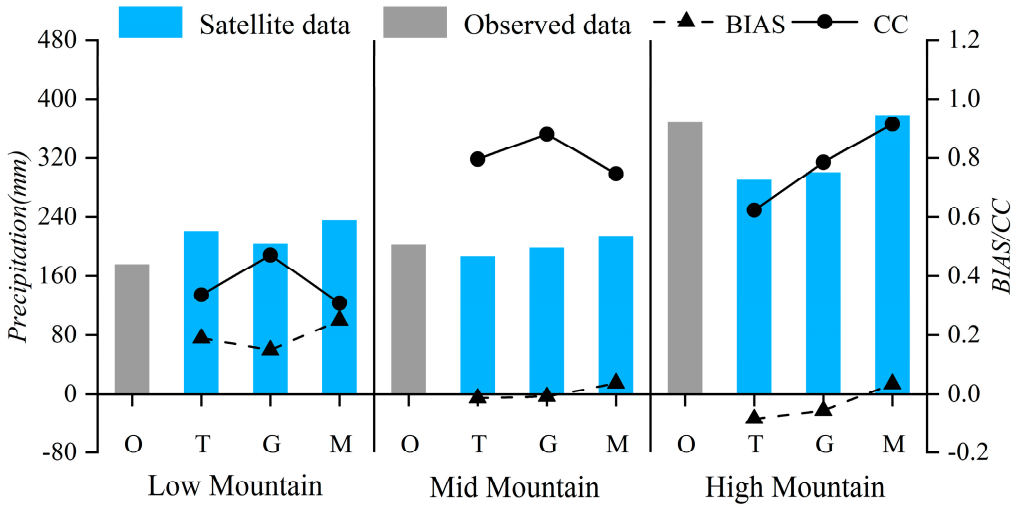

Figure 13. Comparison of average precipitation of three sets of satellite products in different elevation zones. Note: Measured data, TRMM, GPM and MSWEP are in turn from left to right in each elevation zone.

4. Discussion

Tianshan mountain area is characterized by complex topography and landforms and the inherent north–south and east–west heterogeneity of precipitation distribution. Previous studies on the performance evaluation of precipitation products mainly have the following shortcomings: On the one hand, there is no comparison of the limitations of precipitation products from different sources. For example, Guo Hao et al. [73] discussed the role of different satellite precipitation estimation (LSPE) in arid zone climate monitoring, but the mechanism behind the precipitation estimation with different high spatial and temporal resolutions provided by different satellite products was not thoroughly discussed. On the other hand, most of the previous studies used short-term data to evaluate the spatial distribution of precipitation in the Tianshan Mountains. For example, Chi, Zhang [17], and Wu, Lei [72] only compared the applicability of TRMM and GPM products on a short time scale to the inversion of precipitation in The Tianshan Mountains, ignoring the periodicity of precipitation in the high-cold mountains in a long time series and the spatial difference of precipitation in complex terrain. Therefore, this study uses the 20-year observation data of 36 observation stations in four sub-regions of the Tianshan Mountains and nearby areas as samples to study the spatial–temporal performance of three different sources of satellite precipitation estimation products (TRMM, IMERG, and MSWEP) on multiple time scales. The mechanism analysis of different products from different sources and the study of longer time series and hetero-differentiation make our results more convincing than previous research results.

4.1. Accuracy Difference between the Three Products

The results show that the three satellite precipitation products can capture the spatial pattern of precipitation in the Tianshan Mountains at different time scales. However, a common significant weakness of these three precipitation products is that the estimation deviation of the precipitation in the dry season in the Tianshan Mountains is large (Table 2). Ying et al. [98] also found a similar performance of precipitation products in Nepal. TRMM and GPM IMERG are precipitation combination products from IR and PMW sensors, while MSWEP is data from multiple PMW sensors [33]. It is worth mentioning that, on the one hand, the PMW sensor cannot detect a large amount of snow melt water in the dry season; On the other hand, the infrared sensor can not distinguish multi-layer rain clouds in the dry season when there is less rain [33].

The accuracy difference between the three precipitation products is that in the Tianshan Mountains, GPM IMERG is superior to TRMM 3B42 and MSWEP products in cumulative precipitation estimation at all time scales. Although the previous precipitation evaluation in most regions of China showed that the performance of GPM products might be inferior to that of TRMM products in winter [99,100], our study showed that IMERG products performed better than the other two satellite products in precipitation estimation in all seasons, with more balanced seasonal performance (Figure 4). Similarly, studies near the Qinghai Tibet Plateau show that GPM IMERG has significantly better CC and lower BIAS than the previous generation of TRMM3B42 [83]. Like our studies, these studies also found that the detection BIAS of GPM on precipitation has been improved (Figure 5). This improvement is helpful in restoring precipitation in the low mountain and dry land of Central Asia. These improvements can be attributed to the new Ka-band (35.5 GHz) of GPM, which enhances its ability to capture precipitation events [29].

It is worth noting that the results of this study do not indicate that GPM products will be superior to other products in all mountainous areas. A study on precipitation in arid areas found that IMERG did not significantly improve compared with TRMM 3B42 [29]. Although studies in India showed that IMERG was significantly superior to TMPA in detecting heavy monsoon precipitation [64], our study has not found that the ability of GPM to detect daily precipitation events of different intensities in the Tianshan Mountains has been significantly improved (Figure 6) [101]. In fact, TRMM is superior to GPM in

detecting no rain and light rain events in arid areas (Figure 6); MSWEP shows a high level of detection ability for extreme precipitation than GPM (Figure 7), which is consistent with Yuan et al. 's study [29] that 75% of stations' detection results for heavy rain show that GPM products are worse than MSWEP. Previous studies have shown that GPM tends to underestimate convective rain, especially rainstorm accumulation [25]. This weakness limits the effectiveness of GPM in mountainous areas. At the same time, our study shows that the MSWEP product has a better ability to capture the spatial variability of precipitation under complex terrain in the Tianshan mountains than GPM IMERG (Figure 9), which may be related to the fact that MSWEP simultaneously integrates multi-source precipitation data such as ground station precipitation, satellite observation precipitation, and reanalysis data.

4.2. Precipitation Differences in Different Regions of the Tianshan Mountains

Due to the scarcity of station data in high-cold mountains [22,35], this study compared the correlation between station interpolation results and spatial grid data of satellite products to explore the differences in precipitation distribution and the degree of spatial differentiation in different regions of the Tianshan Mountains.

For precipitation in different regions of the Tianshan Mountains, the interpolation results of satellite precipitation products and annual precipitation at observation sites all show similar spatial patterns (Figure 8), that is, a consistent trend of decreasing from north to south and west to east, which is consistent with the research conclusions of Zhang [17], Massari [102], Wei et al. [81]. It fully reflects the spatial differences of precipitation caused by air flow and complex topographic changes in the Tianshan Mountains: Since water vapor in Central Asia mainly comes from westerly circulation, large-scale circulation and the mountain barrier effect form an obvious continental gradient, so the precipitation rate gradually decreases from northwest to southeast [18]. The results of station interpolation and GPM (which is the highest correlation with measured precipitation among the three products) showed that the maximum annual precipitation occurred near the Yili Valley region in the western part of the North Tianshan Mountains (Figure 8a), with annual precipitation exceeding 600 mm. However, the annual precipitation in the East and South regions is basically less than 100 mm, so it is called the "dry pole" of the Tianshan Mountains [77]. This is because the northwest of the mountain area is located on the windward slope of the prevailing westerly wind belt, and the west flow over the troposphere is smooth all year round, leading to more precipitation in the northwest of the mountain area all year round. However, on the leeward south slope, blocked by the mountains, the moisture decreases from west to east. The spatial differentiation degree of precipitation in the Tianshan Mountains is opposite to the spatial distribution of precipitation. Figure 9a shows that although most of the mountains in the West and North regions of the Tianshan Mountains have small precipitation variation (CV < 6%), there are still areas with large inter-annual precipitation variation (CV > 10%) in the East and South regions of the Tianshan Mountains and the desert edge of the Turpan-Hami Basin, which makes water resources management in the eastern region of the Tianshan Mountains more difficult [77]. Of the three products, MSWEP comes closest to this pattern of differentiation (Figure 9d). However, in the wet season, the monsoon circulation from the Pacific and Indian oceans also brings southward water vapor flux, and the difference in precipitation gradient between the North region and South region weakens (Figure 9i) [77].

Our analysis shows that the satellite precipitation products can not only reflect the influence of large-scale circulation on the spatial and temporal patterns of precipitation in the study area but also provide additional evidence for the influence of the topography of different regions in the Tianshan Mountains on the observed precipitation gradients in the Central Asian dryland.

4.3. Application Prospect of Precipitation Products

Due to the sparse distribution of meteorological stations in the Tianshan Mountains, which are mainly distributed in the low mountain area, there may be a large deviation in analyzing precipitation characteristics in the mountainous area only by spatial interpolation of rain gauge data [78]. Therefore, eco-hydrological studies in central Asia, including the Tianshan mountains, must rely on precipitation products as precipitation inputs [101,103]. According to our evaluation results in the Tianshan Mountains, GPM not only has a good correlation with the measured precipitation at different time scales (Section 3.1) but also has a high estimation accuracy for the spatial distribution of precipitation in the mountains (Section 3.2). Previous studies have also shown that, compared with CRP data, precipitation products such as GPM not only have a higher spatial resolution (10 km VS. 40 km) but also have higher accuracy in precipitation estimation in central Asian mountains [19]. The major rivers/lakes in the arid region of Central Asia also depend mainly on the Tianshan Mountains for water. Therefore, as a new generation of precipitation observation satellite, GPM can be used as a meteorological driver for large-scale land surface processes and ecological simulation. At the same time, considering the obvious difference in estimation performance of GPM products under the influence of different terrain factors (Section 3.3), terrain factors can be used to correct them in specific applications so as to improve the accuracy of GPM products.

However, relying on a single precipitation product usually cannot avoid systematic errors caused by its data source [22,24,25]. GPM does not perform as well as MSWEP products in describing precipitation differentiation in mountainous areas (Figure 9) and detecting extreme precipitation events (Figure 7). According to the research of Xuan [32], MSWEP can more scientifically analyze the spatiotemporal variation of precipitation in areas lacking data. In future research work, in addition to evaluating the applicability of precipitation products, it is also necessary to provide a platform with a good spatial and temporal resolution for precipitation prediction and analysis by fusing precipitation products from different sources. For the arid areas in Northwest China with great topographic and geomorphic changes, such as the Tianshan Mountains, we need to combine the existing satellite precipitation products with the topographic and geomorphic factors in the study area to carry out sustainable water resources management and precipitation seasonal forecast [21,32]. By integrating climate forecast (as preliminary forecast), satellite radar precipitation observation (as spatial data), and site measured data (as detection data), combined with topographic and geomorphic data, a multi-scale geographic weighted regression model such as MGWR [78] is used to conduct appropriate deviation correction and construct a precipitation prediction platform. The dataset provided by the precipitation platform can also be used as the background field to cope with drought events or extreme precipitation events.

5. Conclusions

In this study, the precipitation estimation accuracy of TRMM (3B42V7), GPM (IMERGV6), and MSWEP (V2.2) in different regions and time scales in the Tianshan Mountains was systematically evaluated by combining quantitative and categorical evaluation methods. The time series of the study is from 2000 to 2019. In analyzing the results, we also consider the influence of elevation and longitude on the suitability of precipitation products. The main conclusions are as follows:

(1) At the annual scale, the three precipitation products showed a strong correlation with the measured precipitation; During the year, the estimation ability of precipitation in the wet season was stronger than that in the dry season. TRMM showed an underestimation of the measured precipitation, GPM improved the underestimation, and MSWEP showed an overestimation.

(2) At the daily scale, TRMM and MSWEP had the best detection rates for light rain events and extreme precipitation events, respectively. The deviation between GPM and daily precipitation is the smallest.

(3) At the spatial scale, the three precipitation products can roughly reflect the distribution characteristics of the measured precipitation, that is, the trend of decreasing from northwest to southeast, and the correlation between GPM and the measured precipitation is the best. In different regions, the detection rate of precipitation in the West region was the highest, and the detection rate of precipitation in the East region was the worst. MSWEP is the closest to the precipitation differentiation pattern in the Tianshan Mountains.

(4) The three precipitation products showed high accuracy in low longitude areas and middle elevation mountain areas; In comparison, MSWEP has the highest applicability in high-altitude mountain areas.

In general, this study used statistical methods to evaluate the accuracy of three precipitation products in different sub-regions of the Tianshan Mountains and assessed the monitoring ability of precipitation events through categorical analysis. It is found that the GPM precipitation product is the closest to the measured precipitation values at different time scales, and the MSWEP can best reflect the spatial distribution pattern of precipitation in different regions. It is suggested to comprehensively use the estimated values of the two products to understand the precipitation trend in the Tianshan Mountains. This conclusion provides a reference value for multi-source monitoring fusion and multi-source algorithm fusion of data products in the arid mountainous area of Northwest China. At the same time, the deviation analysis of precipitation products also provides a reference for data product developers to improve the precision of products.

Author Contributions: Conceptualization, X.L. (Xiaoqian Li), X.L. (Xiaolong Li), Y.D. and W.X.; Data curation, X.H. and G.Y.; Formal analysis, X.L. (Xiaoqian Li), Y.D. and D.L.; Funding acquisition, X.H. and G.Y.; Investigation, X.L. (Xiaoqian Li), Y.D. and W.X.; Methodology, X.L. (Xiaoqian Li), X.L. (Xiaolong Li) and D.L.; Project administration, X.H.; Resources, X.H. and X.L. (Xiaolong Li); Software, X.L. (Xiaoqian Li), Y.D., D.L. and W.X.; Supervision, X.H., X.L. (Xiaolong Li) and G.Y.; Validation, X.L. (Xiaoqian Li); Visualization, X.L. (Xiaoqian Li) and Y.D.; Writing—original draft, X.L. (Xiaoqian Li); Writing—review and editing, X.H., X.L. (Xiaolong Li) and G.Y. All authors have read and agreed to the published version of the manuscript.

Funding: This research was funded by the third scientific expedition project in Xinjiang (Grant Nos. 2021xjkk0804), Xinjiang Production and Construction Corps scientific and technological break-through project (Grant Nos. 2021AB021), International cooperation and exchange project of Xinjiang production and Construction Corps (Grant Nos. 2022BC001) and the National Natural Science Foundation of China (Grant Nos. U1803244, 51969027), Young talents plan of science and technology think tank in 2022 (20220615ZZ07110104).

Data Availability Statement: The data presented in this study are available on request from the corresponding author.

Acknowledgments: The authors are very grateful to all anonymous reviewers, chief editors and associate editors for their valuable comments and suggestions, which not only greatly improved the quality of this paper but also have immense value for our future research.

Conflicts of Interest: The authors declare no conflict of interest.

Appendix A

Table 1. Precision evaluation indexes of precipitation products.

Index Name	Formula	Ideal Value
Root Mean Square Error (RMSE)	$\mathrm{RMSE} = \sqrt{\frac{\sum_{i=1}^{n}(S_i - G_i)^2}{n}}$	0
Mean Error (ME)	$\mathrm{ME} = \frac{1}{n}\sum_{i=1}^{n}(S_i - G_i)$	0
Mean Absolute Error (MAE)	$\mathrm{MAE} = \frac{1}{n}\sum_{i=1}^{n}(\lvert S_i - G_i \rvert)$	0
Correlation Coefficient (CC)	$\mathrm{CC} = \frac{\sum_{i=1}^{n}(S_i - \bar{S})(G_i - \bar{G})}{\sqrt{\sum_{i=1}^{n}(S_i - \bar{S})^2}\sqrt{\sum_{i=1}^{n}(G_i - \bar{G})^2}}$	1
Frequency Bias (BIAS）	$\mathrm{BIAS} = \frac{\sum_{i=1}^{n}(S_i - G_i)}{\sum_{i=1}^{n} G_i} * 100\%$	0
Probability of Detection (POD)	$\mathrm{POD} = \frac{H}{H + M}$	1
False Alarm Ratio (FAR)	$\mathrm{FAR} = \frac{F}{H + F}$	0
Critical Success Index (CSI)	$\mathrm{CSI} = \frac{H}{H + M + F}$	1
Standard Deviation Ratio (SDR)	$\mathrm{SDR} = \frac{\sqrt{\sum_{i=1}^{n}(S_i - \bar{S})^2}}{\sqrt{\sum_{i=1}^{n}(O_i - \bar{O})^2}}$	1
Coefficient of Variation (CV)	$\mathrm{CV_S} = \frac{\sqrt{\frac{1}{n-1}\sum_{i=1}^{n}(S_i - \bar{S})^2}}{\bar{S}} \times 100\%$ or $\mathrm{CV_G} = \frac{\sqrt{\frac{1}{n-1}\sum_{i=1}^{n}(G_i - \bar{G})^2}}{\bar{G}} \times 100\%$	100

[1] Note: The n is the length of precipitation series; S_i and G_i are TRMM/GPM/MSWEP grid precipitation data and site measured precipitation data respectively. $\bar{S}$ and $\bar{G}$ correspond to the mean values of time series of two precipitation data respectively. H is the number of precipitation events detected simultaneously by precipitation products and ground measured data; M is the number of precipitation events detected by the site but not detected by precipitation products; F refers to the number of precipitation events that are not detected by the station but are falsely reported by precipitation products. In this paper, the threshold of precipitation is determined to be 0.1 mm/day.

Table 2. Name and meaning of extreme climate indices.

Name	Code	Definition	Unit
Consecutive Dry Days	CDD	The longest consecutive days with daily precipitation < 1 mm	d
Consecutive Wet Days	CWD	The longest consecutive days with daily precipitation ≥ 1 mm	d
Simple Daily Precipitation Intensity Index	SDII	The ratio of the total amount of precipitation ≥ 1 mm to the number of days	mm/d^{-1}
Annual Maximum 1-day Precipitation	RX1D	Annual maximum daily precipitation	mm

References

1. Qin, Y.; Chen, Z.; Shen, Y.; Zhang, S.; Shi, R. Evaluation of satellite rainfall estimates over the Chinese Mainland. *Remote Sens.* **2014**, *6*, 11649–11672.
2. Chung, C.T.; Power, S.B.; Arblaster, J.M.; Rashid, H.A.; Roff, G.L. Nonlinear precipitation response to El Niño and global warming in the Indo-Pacific. *Clim. Dyn.* **2014**, *42*, 1837–1856.
3. Nashwan, M.S.; Shahid, S.; Wang, X. Assessment of satellite-based precipitation measurement products over the hot desert climate of Egypt. *Remote Sens.* **2019**, *11*, 555.
4. Chen, C.; Chen, Q.; Duan, Z.; Zhang, J.; Mo, K.; Li, Z.; Tang, G. Multiscale comparative evaluation of the GPM IMERG v5 and TRMM 3B42 v7 precipitation products from 2015 to 2017 over a climate transition area of China. *Remote Sens.* **2018**, *10*, 944.
5. Liang-Liang, L.; Jian, L.; Ru-Cong, Y. Evaluation of CMIP6 HighResMIP models in simulating precipitation over Central Asia. *Adv. Clim. Chang. Res.* **2022**, *13*, 1–13.
6. Siegfried, T.; Bernauer, T.; Guiennet, R.; Sellars, S.; Robertson, A.W.; Mankin, J.; Bauer-Gottwein, P.; Yakovlev, A. Will climate change exacerbate water stress in Central Asia? *Clim. Chang.* **2012**, *112*, 881–899.
7. Xu, M.; Kang, S.; Wu, H.; Yuan, X. Detection of spatio-temporal variability of air temperature and precipitation based on long-term meteorological station observations over Tianshan Mountains, Central Asia. *Atmos. Res.* **2018**, *203*, 141–163.
8. Chen, H.; Chen, Y.; Li, D.; Li, W.; Yang, Y. Identifying water vapor sources of precipitation in forest and grassland in the north slope of the Tianshan Mountains, Central Asia. *J. Arid Land* **2022**, *14*, 297–309.
9. Meng, X.; Long, A.; Wu, Y.; Yin, G.; Wang, H.; Ji, X. Simulation and spatiotemporal pattern of air temperature and precipitation in Eastern Central Asia using RegCM (Retraction of Vol 8, art no 3639, 2018). *Sci. Rep.* **2019**, *18*, 13674.
10. Shi, Y.; Wang, S.; Wang, L.; Zhang, M.; Argiriou, A.A.; Song, Y.; Lei, S. Isotopic evidence in modern precipitation for the westerly meridional movement in Central Asia. *Atmos. Res.* **2021**, *259*, 105698.
11. Xu, X.; Kleidon, A.; Miller, L.; Wang, S.; Wang, L.; Dong, G. Late Quaternary glaciation in the Tianshan and implications for palaeoclimatic change: A review. *Boreas* **2010**, *39*, 215–232.
12. Fan, M.; Xu, J.; Li, D.; Chen, Y. Response of Precipitation in Tianshan to Global Climate Change Based on the Berkeley Earth and ERA5 Reanalysis Products. *Remote Sens.* **2022**, *14*, 519.
13. Yue, X.; Liu, G.; Chen, J.; Zhou, C. Synergistic regulation of the interdecadal variability in summer precipitation over the Tianshan mountains by sea surface temperature anomalies in the high-latitude Northwest Atlantic Ocean and the Mediterranean Sea. *Atmos. Res.* **2020**, *233*, 104717.
14. Cai, P.; Hamdi, R.; Luo, G.; He, H.; Zhang, M.; Termonia, P.; De Maeyer, P. Agriculture intensification increases summer precipitation in Tianshan Mountains, China. *Atmos. Res.* **2019**, *227*, 140–146.
15. Zhang, Q.; Sun, P.; Li, J.; Singh, V.P.; Liu, J. Spatiotemporal properties of droughts and related impacts on agriculture in Xinjiang, China. *Int. J. Climatol.* **2015**, *35*, 1254–1266.
16. Yu, Y.; Chen, X.; Malik, I.; Wistuba, M.; Cao, Y.; Hou, D.; Ta, Z.; He, J.; Zhang, L.; Yu, R. Spatiotemporal changes in water, land use, and ecosystem services in Central Asia considering climate changes and human activities. *J. Arid Land* **2021**, *13*, 881–890.
17. Zhang, C.; Chen, X.; Shao, H.; Chen, S.; Liu, T.; Chen, C.; Ding, Q.; Du, H. Evaluation and intercomparison of high-resolution satellite precipitation estimates—GPM, TRMM, and CMORPH in the Tianshan Mountain Area. *Remote Sens.* **2018**, *10*, 1543.
18. Domrös, M.; Peng, G. *The Climate of China*; Springer Science & Business Media: Berlin/Heidelberg, Germany, 2012.
19. Hu, Z.; Hu, Q.; Zhang, C.; Chen, X.; Li, Q. Evaluation of reanalysis, spatially interpolated and satellite remotely sensed precipitation data sets in central Asia. *J. Geophys. Res. Atmos.* **2016**, *121*, 5648–5663.
20. Dinku, T.; Connor, S.J.; Ceccato, P.; Ropelewski, C.F. Comparison of global gridded precipitation products over a mountainous region of Africa. *Int. J. Climatol. A J. R. Meteorol. Soc.* **2008**, *28*, 1627–1638.
21. Gehne, M.; Hamill, T.M.; Kiladis, G.N.; Trenberth, K.E. Comparison of global precipitation estimates across a range of temporal and spatial scales. *J. Clim.* **2016**, *29*, 7773–7795.
22. Beck, H.E.; Vergopolan, N.; Pan, M.; Levizzani, V.; Van Dijk, A.I.; Weedon, G.P.; Brocca, L.; Pappenberger, F.; Huffman, G.J.; Wood, E.F. Global-scale evaluation of 22 precipitation datasets using gauge observations and hydrological modeling. *Hydrol. Earth Syst. Sci.* **2017**, *21*, 6201–6217.
23. Sadeghi, M.; Nguyen, P.; Naeini, M.R.; Hsu, K.; Braithwaite, D.; Sorooshian, S. PERSIANN-CCS-CDR, a 3-hourly 0.04° global precipitation climate data record for heavy precipitation studies. *Sci. Data* **2021**, *8*, 157.
24. Gebremichael, M.; Anagnostou, E.N.; Bitew, M.M. Critical steps for continuing advancement of satellite rainfall applications for surface hydrology in the Nile River basin 1. *JAWRA J. Am. Water Resour. Assoc.* **2010**, *46*, 361–366.
25. Duan, Y.; Wilson, A.M.; Barros, A.P. Scoping a field experiment: Error diagnostics of TRMM precipitation radar estimates in complex terrain as a basis for IPHEx2014. *Hydrol. Earth Syst. Sci.* **2015**, *19*, 1501–1520.
26. Sun, W.; Sun, Y.; Li, X.; Wang, T.; Wang, Y.; Qiu, Q.; Deng, Z. Evaluation and correction of GPM IMERG precipitation products over the capital circle in Northeast China at multiple spatiotemporal scales. *Adv. Meteorol.* **2018**, *2018*, 4714173.
27. Huffman, G.J.; Bolvin, D.T.; Nelkin, E.J.; Tan, J. Integrated Multi-satellitE Retrievals for GPM (IMERG) technical documentation. *Nasa/Gsfc Code* **2015**, *612*, 2019.
28. Liu, Z. Comparison of integrated multisatellite retrievals for GPM (IMERG) and TRMM multisatellite precipitation analysis (TMPA) monthly precipitation products: Initial results. *J. Hydrometeorol.* **2016**, *17*, 777–790.

29. Yuan, F.; Zhang, L.; Win, K.W.W.; Ren, L.; Zhao, C.; Zhu, Y.; Jiang, S.; Liu, Y. Assessment of GPM and TRMM multi-satellite precipitation products in streamflow simulations in a data-sparse mountainous watershed in Myanmar. *Remote Sens.* **2017**, *9*, 302.
30. Beck, H.E.; Van Dijk, A.I.; Levizzani, V.; Schellekens, J.; Miralles, D.G.; Martens, B.; De Roo, A. MSWEP: 3-hourly 0.25 global gridded precipitation (1979–2015) by merging gauge, satellite, and reanalysis data. *Hydrol. Earth Syst. Sci.* **2017**, *21*, 589–615.
31. Liu, J.; Shangguan, D.; Liu, S.; Ding, Y.; Wang, S.; Wang, X. Evaluation and comparison of CHIRPS and MSWEP daily-precipitation products in the Qinghai-Tibet Plateau during the period of 1981–2015. *Atmos. Res.* **2019**, *230*, 104634.
32. Xuan, D.; Hu, Q.; Wang, Y.; Yang, H.; Li, L.; Wang, L. Precipitation Characteristic Analysis of the Zhoushan Archipelago: From the View of MSWEP and Rainfall Merging. *Water* **2020**, *12*, 829.
33. Yang, Y.; Wu, J.; Bai, L.; Wang, B. Reliability of gridded precipitation products in the Yellow River Basin, China. *Remote Sens.* **2020**, *12*, 374.
34. Li, K.; Tian, F.; Khan, M.Y.A.; Xu, R.; He, Z.; Yang, L.; Lu, H.; Ma, Y. A high-accuracy rainfall dataset by merging multiple satellites and dense gauges over the southern Tibetan Plateau for 2014–2019 warm seasons. *Earth Syst. Sci. Data* **2021**, *13*, 5455–5467.
35. Alijanian, M.; Rakhshandehroo, G.R.; Mishra, A.K.; Dehghani, M. Evaluation of satellite rainfall climatology using CMORPH, PERSIANN-CDR, PERSIANN, TRMM, MSWEP over Iran. *Int. J. Climatol.* **2017**, *37*, 4896–4914.
36. Zhu, Q.; Gao, X.; Xu, Y.-P.; Tian, Y. Merging multi-source precipitation products or merging their simulated hydrological flows to improve streamflow simulation. *Hydrol. Sci. J.* **2019**, *64*, 910–920.
37. Qi, W.; Zhang, C.; Fu, G.; Sweetapple, C.; Zhou, H. Evaluation of global fine-resolution precipitation products and their uncertainty quantification in ensemble discharge simulations. *Hydrol. Earth Syst. Sci.* **2016**, *20*, 903–920.
38. Feng, K.; Hong, Y.; Tian, J.; Luo, X.; Tang, G.; Kan, G. Evaluating applicability of multi-source precipitation datasets for runoff simulation of small watersheds: a case study in the United States. *Eur. J. Remote Sens.* **2021**, *54*, 372–382.
39. Wang, X.; Li, B.; Chen, Y.; Guo, H.; Wang, Y.; Lian, L. Applicability evaluation of multisource satellite precipitation data for hydrological research in arid mountainous areas. *Remote Sens.* **2020**, *12*, 2886.
40. Nepal, B.; Shrestha, D.; Sharma, S.; Shrestha, M.S.; Aryal, D.; Shrestha, N. Assessment of GPM-Era Satellite Products'(IMERG and GSMaP) ability to detect precipitation extremes over mountainous country Nepal. *Atmosphere* **2021**, *12*, 254.
41. Wei, L.; Jiang, S.; Ren, L.; Wang, M.; Zhang, L.; Liu, Y.; Yuan, F.; Yang, X. Evaluation of seventeen satellite-, reanalysis-, and gauge-based precipitation products for drought monitoring across mainland China. *Atmos. Res.* **2021**, *263*, 105813.
42. Hirpa, F.A.; Gebremichael, M.; Hopson, T. Evaluation of high-resolution satellite precipitation products over very complex terrain in Ethiopia. *J. Appl. Meteorol. Climatol.* **2010**, *49*, 1044–1051.
43. Bumke, K. Validation of ERA-Interim precipitation estimates over the Baltic Sea. *Atmosphere* **2016**, *7*, 82.
44. Wang, H.; Zang, F.; Zhao, C.; Liu, C. A GWR downscaling method to reconstruct high-resolution precipitation dataset based on GSMaP-Gauge data: A case study in the Qilian Mountains, Northwest China. *Sci. Total Environ.* **2022**, *810*, 152066.
45. Li, Y.; Qin, X.; Liu, Y.; Jin, Z.; Liu, J.; Wang, L.; Chen, J. Evaluation of Long-Term and High-Resolution Gridded Precipitation and Temperature Products in the Qilian Mountains, Qinghai–Tibet Plateau. *Front. Environ. Sci.* **2022**, *609*, 906821.
46. Kumar, M.; Hodnebrog, Ø.; Daloz, A.S.; Sen, S.; Badiger, S.; Krishnaswamy, J. Measuring precipitation in Eastern Himalaya: Ground validation of eleven satellite, model and gauge interpolated gridded products. *J. Hydrol.* **2021**, *599*, 126252.
47. Hamm, A.; Arndt, A.; Kolbe, C.; Wang, X.; Thies, B.; Boyko, O.; Reggiani, P.; Scherer, D.; Bendix, J.; Schneider, C. Intercomparison of gridded precipitation datasets over a sub-region of the Central Himalaya and the Southwestern Tibetan Plateau. *Water* **2020**, *12*, 3271.
48. Zhang, M.; Luo, G.; De Maeyer, P.; Cai, P.; Kurban, A. Improved atmospheric modelling of the oasis-desert system in Central Asia using WRF with actual satellite products. *Remote Sens.* **2017**, *9*, 1273.
49. Lu, X.-y.; Chen, Y.-y.; Tang, G.-q.; Wang, X.-q.; Liu, Y.; Wei, M. Quantitative estimation of hourly precipitation in the Tianshan Mountains based on area-to-point kriging downscaling and satellite-gauge data merging. *J. Mt. Sci.* **2022**, *19*, 58–72.
50. Zhang, Y.; Hanati, G.; Danierhan, S.; Liu, Q.; Xu, Z. Evaluation and comparison of daily GPM/TRMM precipitation products over the Tianshan Mountains in China. *Water* **2020**, *12*, 3088.
51. Anjum, M.N.; Ahmad, I.; Ding, Y.; Shangguan, D.; Zaman, M.; Ijaz, M.W.; Sarwar, K.; Han, H.; Yang, M. Assessment of IMERG-V06 precipitation product over different hydro-climatic regimes in the Tianshan Mountains, North-Western China. *Remote Sens.* **2019**, *11*, 2314.
52. Yang, M.; Li, Z.; Anjum, M.N.; Gao, Y. Performance Evaluation of Version 5 (V05) of Integrated Multi-Satellite Retrievals for Global Precipitation Measurement (IMERG) over the Tianshan Mountains of China. *Water* **2019**, *11*, 1139.
53. Guo, H.; Chen, S.; Bao, A.; Hu, J.; Gebregiorgis, A.S.; Xue, X.; Zhang, X. Inter-comparison of high-resolution satellite precipitation products over Central Asia. *Remote Sens.* **2015**, *7*, 7181–7211.
54. Lu, X.; Tang, G.; Wei, M.; Yang, L.; Zhang, Y. Evaluation of multi-satellite precipitation products in Xinjiang, China. *Int. J. Remote Sens.* **2018**, *39*, 7437–7462.
55. Palazzi, E.; Von Hardenberg, J.; Provenzale, A. Precipitation in the Hindu-Kush Karakoram Himalaya: observations and future scenarios. *J. Geophys. Res. Atmos.* **2013**, *118*, 85–100.
56. Ji, X.; Chen, Y. Characterizing spatial patterns of precipitation based on corrected TRMM 3B43 data over the mid Tianshan Mountains of China. *J. Mt. Sci.* **2012**, *9*, 628–645.

57. Zhao, C.; Yao, S.; Zhang, S.; Han, H.; Zhao, Q.; Yi, S. Validation of the accuracy of different precipitation datasets over Tianshan mountainous area. *Adv. Meteorol.* **2015**, *2015*, 617382.
58. Fan, M.; Xu, J.; Chen, Y.; Li, W. Simulating the precipitation in the data-scarce Tianshan Mountains, Northwest China based on the Earth system data products. *Arab. J. Geosci.* **2020**, *13*, 637.
59. Zhengyong, Z.; Xinlin, H.; Lin, L.; Zhongqin, L.; Puyu, W. Spatial distribution of rainfall simulation and the cause analysis in China's Tianshan Mountains area. *Adv. Water Sci.* **2015**, *26*, 500–508.
60. Kummerow, C.; Simpson, J.; Thiele, O.; Barnes, W.; Chang, A.; Stocker, E.; Adler, R.; Hou, A.; Kakar, R.; Wentz, F. The status of the Tropical Rainfall Measuring Mission (TRMM) after two years in orbit. *J. Appl. Meteorol.* **2000**, *39*, 1965–1982.
61. Sharifi, E.; Eitzinger, J.; Dorigo, W. Performance of the state-of-the-art gridded precipitation products over mountainous terrain: A regional study over Austria. *Remote Sens.* **2019**, *11*, 2018.
62. Jiang, H.; Zipser, E.J. Contribution of tropical cyclones to the global precipitation from eight seasons of TRMM data: Regional, seasonal, and interannual variations. *J. Clim.* **2010**, *23*, 1526–1543.
63. Scheel, M.; Rohrer, M.; Huggel, C.; Santos Villar, D.; Silvestre, E.; Huffman, G. Evaluation of TRMM Multi-satellite Precipitation Analysis (TMPA) performance in the Central Andes region and its dependency on spatial and temporal resolution. *Hydrol. Earth Syst. Sci.* **2011**, *15*, 2649–2663.
64. Sharifi, E.; Steinacker, R.; Saghafian, B. Assessment of GPM-IMERG and other precipitation products against gauge data under different topographic and climatic conditions in Iran: Preliminary results. *Remote Sens.* **2016**, *8*, 135.
65. Li, Y.; Feng, A.; Liu, W.; Ma, X.; Dong, G. Variation of aridity index and the role of climate variables in the Southwest China. *Water* **2017**, *9*, 743.
66. Liu, X.; Yang, T.; Hsu, K.; Liu, C.; Sorooshian, S. Evaluating the streamflow simulation capability of PERSIANN-CDR daily rainfall products in two river basins on the Tibetan Plateau. *Hydrol. Earth Syst. Sci.* **2017**, *21*, 169–181.
67. Huang, Y.; Chen, S.; Cao, Q.; Hong, Y.; Wu, B.; Huang, M.; Qiao, L.; Zhang, Z.; Li, Z.; Li, W. Evaluation of version-7 TRMM multi-satellite precipitation analysis product during the Beijing extreme heavy rainfall event of 21 July 2012. *Water* **2013**, *6*, 32–44.
68. Ulloa, J.; Ballari, D.; Campozano, L.; Samaniego, E. Two-step downscaling of TRMM 3B43 V7 precipitation in contrasting climatic regions with sparse monitoring: The case of Ecuador in tropical South America. *Remote Sens.* **2017**, *9*, 758.
69. Price, D.T.; McKenney, D.W.; Nalder, I.A.; Hutchinson, M.F.; Kesteven, J.L. A comparison of two statistical methods for spatial interpolation of Canadian monthly mean climate data. *Agric. For. Meteorol.* **2000**, *101*, 81–94.
70. Cressie, N.; Sainsbury-Dale, M.; Zammit-Mangion, A. Basis-Function Models in Spatial Statistics. *arXiv* **2022**, *arXiv*:2202.03660.
71. Johannesson, G.; Cressie, N. Finding large-scale spatial trends in massive, global, environmental datasets. *Env. Off. J. Int. Env. Soc.* **2004**, *15*, 1–44.
72. Simeng, W.; Dazhao, W.; Chang, H. A comparative study of using ANUSPLIN and GWR models for downscaled GPM precipitation. In Proceedings of the 2019 8th International Conference on Agro-Geoinformatics (Agro-Geoinformatics), Istanbul, Turkey, 16–19 July 2019; pp. 1–5.
73. Guo, B.; Zhang, J.; Meng, X.; Xu, T.; Song, Y. Long-term spatio-temporal precipitation variations in China with precipitation surface interpolated by ANUSPLIN. *Sci. Rep.* **2020**, *10*, 81.
74. Shu, S.; Liu, C.; Shi, R.; Gao, W. Research on spatial interpolation of meteorological elements in Anhui Province based on ANUSPLIN. In Proceedings of the Remote Sensing and Modeling of Ecosystems for Sustainability VIII, San Diego, CA, USA, 15 September 2011; pp. 183–194.
75. An, Y.; Zhao, W.; Li, C.; Liu, Y. Evaluation of six satellite and reanalysis precipitation products using gauge observations over the Yellow River Basin, China. *Atmosphere* **2020**, *11*, 1223.
76. Vincent, L.A.; Peterson, T.; Barros, V.; Marino, M.; Rusticucci, M.; Carrasco, G.; Ramirez, E.; Alves, L.; Ambrizzi, T.; Berlato, M. Observed trends in indices of daily temperature extremes in South America 1960–2000. *J. Clim.* **2005**, *18*, 5011–5023.
77. Sorg, A.; Bolch, T.; Stoffel, M.; Solomina, O.; Beniston, M. Climate change impacts on glaciers and runoff in Tien Shan (Central Asia). *Nat. Clim. Chang.* **2012**, *2*, 725–731.
78. Michaelides, S.; Levizzani, V.; Anagnostou, E.; Bauer, P.; Kasparis, T.; Lane, J.E. Precipitation: Measurement, remote sensing, climatology and modeling. *Atmos. Res.* **2009**, *94*, 512–533.
79. Sun, W.; Mu, X.; Song, X.; Wu, D.; Cheng, A.; Qiu, B. Changes in extreme temperature and precipitation events in the Loess Plateau (China) during 1960–2013 under global warming. *Atmos. Res.* **2016**, *168*, 33–48.
80. Rahimzadeh, F.; Asgari, A.; Fattahi, E. Variability of extreme temperature and precipitation in Iran during recent decades. *Int. J. Climatol. A J. R. Meteorol. Soc.* **2009**, *29*, 329–343.
81. Li, W.; Jiang, Z.; Zhang, X.; Li, L.; Sun, Y. Additional risk in extreme precipitation in China from 1.5 °C to 2.0 °C global warming levels. *Sci. Bull.* **2018**, *63*, 228–234.
82. Zambrano-Bigiarini, M.; Nauditt, A.; Birkel, C.; Verbist, K.; Ribbe, L. Temporal and spatial evaluation of satellite-based rainfall estimates across the complex topographical and climatic gradients of Chile. *Hydrol. Earth Syst. Sci.* **2017**, *21*, 1295–1320.
83. Sharifi, E.; Steinacker, R.; Saghafian, B. Multi time-scale evaluation of high-resolution satellite-based precipitation products over northeast of Austria. *Atmos. Res.* **2018**, *206*, 46–63.
84. Samel, A.N.; Wang, S.; Wang, W.-C. A comparison between observed and GCM-simulated summer monsoon characteristics over China. *J. Clim.* **1995**, *8*, 1690–1696.

85. Ni, F.; Cavazos, T.; Hughes, M.K.; Comrie, A.C.; Funkhouser, G. Cool-season precipitation in the southwestern USA since AD 1000: Comparison of linear and nonlinear techniques for reconstruction. *Int. J. Climatol. A J. R. Meteorol. Soc.* **2002**, *22*, 1645–1662.
86. Zhang, X.; Alexander, L.; Hegerl, G.C.; Jones, P.; Tank, A.K.; Peterson, T.C.; Trewin, B.; Zwiers, F.W. Indices for monitoring changes in extremes based on daily temperature and precipitation data. *Wiley Interdiscip. Rev. Clim. Chang.* **2011**, *2*, 851–870.
87. Kao, S.-C.; Govindaraju, R.S. A copula-based joint deficit index for droughts. *J. Hydrol.* **2010**, *380*, 121–134.
88. Taylor, K.E. Summarizing multiple aspects of model performance in a single diagram. *J. Geophys. Res. Atmos.* **2001**, *106*, 7183–7192.
89. Nakamura, K. Progress from TRMM to GPM. *J. Meteorol. Soc. Jp. Ser. II* **2021**, *99*, 697–729.
90. Zhang, Q.; Singh, V.P.; Li, J.; Jiang, F.; Bai, Y. Spatio-temporal variations of precipitation extremes in Xinjiang, China. *J. Hydrol.* **2012**, *434*, 7–18.
91. Lv, A.; Qi, S.; Wang, G. Multi-model driven by diverse precipitation datasets increases confidence in identifying dominant factors for runoff change in a subbasin of the Qaidam Basin of China. *Sci. Total Environ.* **2022**, *802*, 149831.
92. Almazroui, M.; Islam, M.N.; Dambul, R.; Jones, P. Trends of temperature extremes in Saudi Arabia. *Int. J. Climatol.* **2014**, *34*, 808–826.
93. Mitchell, T.D.; Jones, P.D. An improved method of constructing a database of monthly climate observations and associated high-resolution grids. *Int. J. Climatol. A J. R. Meteorol. Soc.* **2005**, *25*, 693–712.
94. Salio, P.; Hobouchian, M.P.; Skabar, Y.G.; Vila, D. Evaluation of high-resolution satellite precipitation estimates over southern South America using a dense rain gauge network. *Atmos. Res.* **2015**, *163*, 146–161.
95. Sun, Q.; Miao, C.; Duan, Q.; Ashouri, H.; Sorooshian, S.; Hsu, K.L. A review of global precipitation data sets: Data sources, estimation, and intercomparisons. *Rev. Geophys.* **2018**, *56*, 79–107.
96. Prakash, S.; Mitra, A.K.; Pai, D.; AghaKouchak, A. From TRMM to GPM: How well can heavy rainfall be detected from space? *Adv. Water Resour.* **2016**, *88*, 1–7.
97. Kumari, M.; Singh, C.K.; Bakimchandra, O.; Basistha, A. DEM-based delineation for improving geostatistical interpolation of rainfall in mountainous region of Central Himalayas, India. *Theor. Appl. Climatol.* **2017**, *130*, 51–58.
98. Yin, G.; Chen, X.; Tiyip, T. A comparison study between site-extrapolation-based and regional climate model-simulated climate datasets. *Adv. Water Sci.* **2015**, *26*, 631–643.
99. Guo, H.; Chen, S.; Bao, A.; Behrangi, A.; Hong, Y.; Ndayisaba, F.; Hu, J.; Stepanian, P.M. Early assessment of integrated multi-satellite retrievals for global precipitation measurement over China. *Atmos. Res.* **2016**, *176*, 121–133.
100. Tang, G.; Ma, Y.; Long, D.; Zhong, L.; Hong, Y. Evaluation of GPM Day-1 IMERG and TMPA Version-7 legacy products over Mainland China at multiple spatiotemporal scales. *J. Hydrol.* **2016**, *533*, 152–167.
101. Liu, C.; Zipser, E.J. The global distribution of largest, deepest, and most intense precipitation systems. *Geophys. Res. Lett.* **2015**, *42*, 3591–3595.
102. Massari, C.; Crow, W.; Brocca, L. An assessment of the performance of global rainfall estimates without ground-based observations. *Hydrol. Earth Syst. Sci.* **2017**, *21*, 4347–4361.
103. Zhou, C.; Gao, W.; Hu, J.; Du, L.; Du, L. Capability of imerg v6 early, late, and final precipitation products for monitoring extreme precipitation events. *Remote Sensing*. **2021**,*13*, 689.